https://doi.org/10.5194/egusphere-2022-1340
Preprint. Discussion started: 2 December 2022

Interactions between ocean heat budget terms in HighResMIP climate models measured by the rate of information transfer

David Docquier[1], Stéphane Vannitsem[1], Alessio Bellucci[2], and Claude Frankignoul[3,4]

[1]Royal Meteorological Institute of Belgium, Brussels, Belgium
[2]Italian National Research Council, Institute of Atmospheric Sciences and Climate (CNR-ISAC), Bologna, Italy
[3]Sorbonne University, Paris, France
[4]Woods Hole Oceanographic Institution, Woods Hole, United States

Correspondence: D. Docquier (david.docquier@meteo.be)

Abstract. The Liang-Kleeman rate of information transfer is used to quantify interactions between the different terms of the ocean heat budget at monthly time scale over the period 1988-2017 in three coupled global climate models participating in the High Resolution Model Intercomparison Project (HighResMIP), as well as in the Ocean Reanalysis System 5 (ORAS5). In particular, we focus on the influences of ocean heat transport convergence (dynamical influence) and net surface heat flux (thermodynamical influence) on ocean heat content tendency. At least two different configurations are used for each model, allowing to investigate the impact of ocean resolution on these causal relationships. A very small number of regions with a dynamical influence is found at high ocean resolution ($\leq 0.25°$) and ORAS5 reanalysis when considering the upper 50 m, while a thermodynamical influence is present in a large number of regions. The number of regions with a dynamical influence increases when taking into account the upper 300 m and becomes comparable to the thermodynamical influence. Interestingly, low-resolution model configurations (1° in the ocean) show a much larger number of regions with a significant dynamical influence for both depth integrations (upper 50 m and 300 m) compared to high-resolution model configurations. The reason for the large difference in dynamical influence between low and high resolutions partly comes from the spatial distribution of ocean velocity field, which is highly variable at high resolution, leading to a smaller dynamical influence. High resolution is therefore key in representing realistically the causal interactions between the ocean and atmosphere.

1 Introduction

The climate on Earth is strongly affected by energy exchanges between the ocean and atmosphere, as the ocean covers more than 70% of the Earth surface and absorbs a major part of the incoming energy. The global energy imbalance between 1971 and 2018 amounts to 0.57 W m^{-2}, with the ocean heat uptake contributing to 91% of the total energy change (Forster et al., 2021). The energy absorbed by the ocean is stored as heat, with more than half of that heat in the upper 700 m (Forster et al., 2021). The ocean plays a key role in redistributing this heat from equatorial regions, where it takes up heat in excess, to higher latitudes, where heat gets released to the atmosphere (Trenberth and Caron, 2001). Understanding whether variations in ocean heat content (OHC) are driven by air-sea heat fluxes or by ocean dynamics is of crucial importance to enhance climate predictions and projections (Roberts et al., 2017).

https://doi.org/10.5194/egusphere-2022-1340
Preprint. Discussion started: 2 December 2022

Several studies have focused on a budget-based approach to evaluate the drivers of OHC variability. Buckley et al. (2014) analyzed processes driving variations in upper OHC (down to the winter mixed layer depth) in the North Atlantic using a data assimilating ocean model coming from Estimating the Circulation and Climate of the Ocean (ECCO) project (ocean resolution of 1°). They found that while OHC tendency is predominantly explained by local (air-sea heat flux and Ekman) forcing in the subtropical gyre at all considered time scales (monthly to decadal), geostrophic heat transport convergence plays a major role in the Gulf Stream region at time scales longer than 6 months. Roberts et al. (2017) combined four surface heat flux reanalysis products with the EN4 OHC dataset (inferring ocean heat transport convergence as a residual) on a common 1° grid and identified regions where ocean dynamics and local air-sea fluxes drive the ocean heat budget at interannual time scales over 1985-2012. They found that ocean heat transport (OHT) convergence dominates variations in OHC in the mixed layer in equatorial regions and regions of strong ocean currents, while OHC is controlled more by net surface heat flux (Qnet) in subtropical gyres and subpolar gyres of the North Atlantic and North Pacific. Over the full depth, variations in OHT convergence dominate changes in OHC in most regions of the world. Small et al. (2020) used version 4 of the Community Climate System Model (CCSM4) at both low (0.5° in the atmosphere and 1° in the ocean) and high (0.25° in the atmosphere and 0.1° in the ocean) resolutions over a 10-year and an 8-year control run, respectively, and analyzed results at monthly time scales. They found that in the upper 50 m and at low resolution, OHC tendency is mainly driven by Qnet over large regions of the globe, except in the eastern tropical Pacific and Atlantic. In contrast, OHC tendency is dominated by OHT convergence at high resolution. The influence of OHT convergence on OHC tendency increases when integrating over deeper depths (upper 400 m) at both low and high resolutions.

The above-mentioned studies mainly used variance, correlation and regression analyses. However, the presence of statistically significant correlations does not firmly demonstrate causal influences between variables, as correlation does not necessarily imply causation. In order to identify causal links, several causal inference frameworks have been developed (Granger, 1969; Schreiber, 2000; Sugihara et al., 2012; Liang and Kleeman, 2005; Krakovská et al., 2018; Palûs et al., 2018; Runge et al., 2019). The Liang-Kleeman information flow method (Liang and Kleeman, 2005) is particularly interesting because it allows for identifying the direction and magnitude of the cause-effect relationships between variables. It is based on the rate of information transfer in dynamical systems; it has initially been developed for two-variable systems (Liang, 2014) and has recently been extended to multivariate systems (Liang, 2021). This novel method has been successfully applied in several climate studies, e.g. causal influences between greenhouse gases and global mean surface temperature (Stips et al., 2016; Jiang et al., 2019), the dynamical dependence between a set of observables and the Antarctic surface mass balance (Vannitsem et al., 2019), soil moisture - air temperature interactions in China (Hagan et al., 2019), prediction of El Niño Modoki (Liang et al., 2021), causal links between climate indices in the North Pacific and Atlantic regions (Vannitsem and Liang, 2022), identification of potential drivers of Arctic sea-ice changes (Docquier et al., 2022b), and ocean-atmosphere interactions (Docquier et al., 2022a).

In our study, we analyze the causal influences between the different terms of the ocean heat budget using the multivariate approach of the rate of information transfer developed by Liang (2021). This allows to check the relative contribution of dynamical (represented by OHT convergence) and thermodynamical (represented by Qnet) influences on changes in OHC.

https://doi.org/10.5194/egusphere-2022-1340
Preprint. Discussion started: 2 December 2022

Our analysis goes beyond previous studies (Buckley et al., 2014; Roberts et al., 2017; Small et al., 2020), which have mainly used correlation and regression analyses between the different ocean heat budget terms, potentially including non-causal relationships. We use three different global climate models participating in the High Resolution Model Intercomparison Project (HighResMIP) with at least two different configurations, which allows for investigating the role of ocean resolution. Model-based results are further validated through the use of the ORAS5 reanalysis, as an observational surrogate. Section 2 presents the data and methods used in this analysis. Section 3 provides the main results of our study and places them in the overall context. Our conclusions are presented in Sect. 4.

2 Data and Methods

2.1 Data

Three different global coupled climate models are used: (1) the European Community Earth-System Model version 3 (EC-Earth3; Haarsma et al. 2020), (2) the Hadley Centre Global Environment Model 3 - Global Coupled version 3.1 (HadGEM3-GC3.1, hereafter referred to as HadGEM3; Roberts et al. 2019), and (3) the Community Earth System Model version 1 (CESM1; Meehl et al. 2019). We use at least two different configurations for each model that mainly differ by their spatial horizontal resolution (in the atmosphere and ocean), including a total of eight model configurations (Table 1). They all follow the High Resolution Model Intercomparison Project (HighResMIP) protocol (Haarsma et al., 2016). We use historical simulations ('hist-1950') for 1988-2014 and future simulations ('highres-future') for 2015-2017. We extract monthly mean ocean potential temperature, zonal and meridional ocean velocities, surface shortwave and longwave radiations, and latent and sensible heat fluxes from the first member of each model.

EC-Earth3 is composed of the Integrated Forecasting System (IFS) atmosphere model, cycle 36r4, and version 3.6 of the Nucleus for European Modeling of the Ocean (NEMO3.6; Madec et al. 2017). The low-resolution configuration, EC-Earth3P (hereafter referred to as EC-Earth3-LR), uses the T255 atmosphere grid (nominal resolution of 100 km) and ORCA1 ocean grid (nominal resolution of 1°, i.e. ∼100 km). The high-resolution configuration, EC-Earth3P-HR (hereafter referred to as EC-Earth3-HR), uses the T511 atmosphere grid (nominal resolution of 50 km) and ORCA025 ocean grid (nominal resolution of 0.25°, i.e. ∼25 km).

HadGEM3 includes the Global Atmosphere 7.1 configuration (GA7.1; Walters et al. 2019) of the Met Office Unified Model (MetUM) and the NEMO3.6 ocean model. Four different configurations of HadGEM3 are used and mainly differ by their spatial resolution. HadGEM3-GC3.1-LL (hereafter referred to as HadGEM3-LL) uses the N96 atmosphere grid (nominal resolution of 250 km) and ORCA1 ocean grid (nominal resolution of 1°, i.e. ∼100 km). HadGEM3-GC3.1-MM (hereafter referred to as HadGEM3-MM) uses the N216 atmosphere grid (nominal resolution of 100 km) and ORCA025 ocean grid (nominal resolution of 0.25°, i.e. ∼25 km). HadGEM3-GC3.1-HM (hereafter referred to as HadGEM3-HM) uses the N512 atmosphere grid (nominal resolution of 50 km) and has the same ocean resolution as HadGEM3-MM (0.25°). HadGEM3-GC3.1-HH (hereafter referred to as HadGEM3-HH) uses the same atmosphere resolution as HadGEM3-HM (50 km) and ORCA12 ocean grid (nominal resolution of 1/12°, i.e. ∼8 km).

https://doi.org/10.5194/egusphere-2022-1340
Preprint. Discussion started: 2 December 2022

Table 1. Model configurations and reanalysis used in this study, together with their atmospheric and ocean model components and nominal resolutions (approximate resolutions at 50°N are provided in parenthesis). The full model names are provided in parenthesis and italics below the names used in this study.

Dataset	Atm. model / forcing	Atm. resolution	Ocean model	Ocean resolution	References
Models					
1. EC-Earth3-LR *(EC-Earth3P)*	IFS cy36r4	100 km (70 km)	NEMO3.6	100 km (70 km)	Haarsma et al. (2020), EC-Earth-Consortium (2019)
2. EC-Earth3-HR *(EC-Earth3P-HR)*	IFS cy36r4	50 km (40 km)	NEMO3.6	25 km (20 km)	Haarsma et al. (2020), EC-Earth-Consortium (2018)
3. HadGEM3-LL *(HadGEM3-GC3.1-LL)*	MetUM	250 km (135 km)	NEMO3.6	100 km (70 km)	Roberts et al. (2019), Roberts (2017a)
4. HadGEM3-MM *(HadGEM3-GC3.1-MM)*	MetUM	100 km (60 km)	NEMO3.6	25 km (20 km)	Roberts et al. (2019), Roberts (2017b)
5. HadGEM3-HM *(HadGEM3-GC3.1-HM)*	MetUM	50 km (25 km)	NEMO3.6	25 km (20 km)	Roberts et al. (2019), Roberts (2017c)
6. HadGEM3-HH *(HadGEM3-GC3.1-HH)*	MetUM	50 km (25 km)	NEMO3.6	8 km (6 km)	Roberts et al. (2019), Roberts (2018)
7. CESM1-LR *(CESM1-CAM5-SE-LR)*	CAM5.2	100 km (60 km)	POP2	100 km (80 km)	Meehl et al. (2019), Hurrell et al. (2020a)
8. CESM1-HR *(CESM1-CAM5-SE-HR)*	CAM5.2	25 km (20 km)	POP2	10 km (8 km)	Meehl et al. (2019), Hurrell et al. (2020b)
Reanalysis					
ORAS5	Forcing: ERA-Interim	100 km (70 km)	NEMO3.4	25 km (20 km)	Zuo et al. (2019)

CESM1 is composed of the Community Atmosphere Model 5.2 (CAM5.2; Park et al. 2014) and the Parallel Ocean Program 2 (POP2; Smith et al. 2010). The low-resolution configuration, CESM1-CAM5-SE-LR (hereafter referrered to as CESM1-LR), employs a nominal resolution of 1° (i.e. ∼100 km) in both the atmosphere and ocean. The high-resolution configuration, CESM1-CAM5-SE-HR (hereafter referred to as CESM1-HR), employs a nominal resolution of 0.25° (i.e. ∼25 km) in the atmosphere and 0.1° (i.e. ∼10 km) in the ocean.

We use the terminology 'low resolution' for model configurations having an ocean resolution of 1° (i.e. EC-Earth3-LR, HadGEM3-LL and CESM1-LR), and 'high resolution' for model configurations that have an ocean resolution finer than, or equal to 0.25° (i.e. EC-Earth3-HR, HadGEM3-MM, HadGEM3-HM, HadGEM3-HH and CESM1-HR).

We finally make use of the Ocean Reanalysis System 5 product (ORAS5) released by the European Centre for Medium-Range Weather Forecasts (ECMWF) OCEAN5 global eddy-permitting ocean and sea-ice ensemble reanalysis system at a resolution of 0.25° (Table 1; Zuo et al. 2019), comparable to high-resolution model configurations. The ocean and sea-ice

https://doi.org/10.5194/egusphere-2022-1340
Preprint. Discussion started: 2 December 2022

components are NEMO3.4 (Madec, 2008) and LIM2 (Fichefet and Morales Maqueda, 1997). In our study, we use the first ORAS5 member (out of five members), which is the control (unperturbed) member, initialized using the ECMWF Reanalysis - 40 years (ERA40) from 1958 to 1979. The atmospheric forcing is ERA-Interim from 1979 to 2015, and the ECMWF operational numerical weather prediction model thereafter. ORAS5 assimilates sea-surface temperature (SST), sea-ice concentration and ocean temperature and salinity from different products that are described in Zuo et al. (2019). Data are available from 1979, and we extract monthly mean ocean potential temperature, zonal and meridional ocean velocities, as well as net downward heat flux.

In our study, monthly data covering the period 1988-2017 are used for all model and reanalysis datasets. This period provides a total of 360 months, which is sufficient to apply the information flow method (Sect. 2.2). This specific period has also been chosen to be able to directly compare results to a previous analysis using the rate of information transfer applied to satellite observations (Docquier et al., 2022a). In order to check the robustness of results related to the length of the time period, monthly data from a 100-year-long HighResMIP control simulation ('control-1950') with EC-Earth3-HR have also been used.

2.2 Methods

Our analysis is conducted on the three main terms of the ocean heat budget, namely ocean heat content (OHC) tendency, ocean heat transport (OHT) convergence and net atmospheric surface heat flux (Qnet), based on the studies from Buckley et al. (2014), Roberts et al. (2017) and Small et al. (2020). The main novelty compared to these previous analyses is the computation of causal influences between ocean heat budget terms (see below).

Two different depth integrations are chosen for the computation of OHC tendency and OHT convergence in order to quantify causal influences in a context dominated by mixed layer processes (upper 50 m) and in another one where we take into account processes that occur generally deeper than the mixed layer (upper 300 m; with the exception of the northern North Atlantic and sub-Antarctic frontal zone in winter; de Boyer Montégut et al. 2004), in a similar way as Small et al. (2020). More precisely, we use the upper 47 m and 301 m for NEMO-based models and reanalysis (EC-Earth3, HadGEM3 and ORAS5), and the upper 55 m and 306 m for CESM1, accounting for the different vertical grid spacing of the analyzed ocean model components.

OHC in each grid point (expressed in J m^{-2}) is computed via the depth integration of ocean potential temperature T over the upper 50 m or upper 300 m of the ocean:

$$OHC = \rho c_p \int T dz, \tag{1}$$

where ρ is the seawater density (ρ = 1027 kg m^{-3}), c_p is the specific seawater heat capacity (c_p = 3985 J kg^{-1} K^{-1}), z is the depth. OHC tendency is computed via a central difference approximation scheme using a time step of one month and is expressed in W m^{-2}.

OHT convergence (expressed in W m^{-2}) is the opposite of OHT divergence ($\nabla \cdot$ OHT), which is computed at each grid point as the depth integration of the divergence in the product of ocean temperature and ocean velocity over the upper 50 m or upper 300 m of the ocean:

$$\nabla \cdot OHT = \rho c_p \int \nabla \cdot \mathbf{U}(T - T_{ref}) dz, \tag{2}$$

https://doi.org/10.5194/egusphere-2022-1340
Preprint. Discussion started: 2 December 2022

where $\mathbf{U}$ is the ocean horizontal velocity vector and T_{ref} is the reference temperature (set to 0°C). The divergence in the product of temperature and velocity is computed via a central difference approximation scheme using a time step of one month. Note that in Roberts et al. (2017), OHT convergence is estimated as a residual, while we compute it directly from monthly temperature and velocity data.

Qnet is computed as the sum of all shortwave and longwave radiation fluxes at the surface as well as latent and sensible heat fluxes. Note that for ORAS5, Qnet is directly provided as an output. All fluxes are expressed in W m^{-2} and are positive downwards.

At each grid point, we compute the rate of information transfer between OHC tendency, OHT convergence and Qnet. As for each pair of variables, the rate of information is computed in the two directions, this results in six different causal relationships. We reproduce this computation for every grid point of the globe over the period 1988-2017. For climate models, we interpolate OHC tendency and OHT convergence onto the atmosphere grid before calculating the rate of information transfer. As the information flow method applies to stationary time series (Liang, 2021; Docquier et al., 2022b), we remove the trend and seasonality of all three variables using a linear regression and additive decomposition. In our analysis, we focus on two specific causal relationships, i.e. the (dynamical) influence of OHT convergence on OHC tendency and the (thermodynamical) influence of Qnet on OHC tendency.

The absolute rate of information transfer from variable X_j to variable X_i is computed assuming linearity following Liang (2021):

$$T_{j\rightarrow i} = \frac{1}{\det\mathbf{C}} \cdot \sum_{k=1}^{d} \Delta_{jk} C_{k,di} \cdot \frac{C_{ij}}{C_{ii}}, \tag{3}$$

where $\mathbf{C}$ is the covariance matrix, d is the number of variables (d = 3 in our case), Δ_{jk} are the cofactors of $\mathbf{C}$, $C_{k,di}$ is the sample covariance between all X_k and the Euler forward difference approximation of dX_i/dt (dt is the one-month time step), C_{ij} is the sample covariance between X_i and X_j, C_{ii} is the sample variance of X_i.

To assess the importance of the different cause-effect relationships, we compute the relative rate of information transfer from variable X_j to variable X_i following the normalization procedure of Liang (2021):

$$\tau_{j\rightarrow i} = \frac{T_{j\rightarrow i}}{Z_i}, \tag{4}$$

where Z_i is the normalizer, computed as follows:

$$Z_i = \sum_{k=1}^{d} |T_{k\rightarrow i}| + \left| \frac{dH_i^{noise}}{dt} \right|, \tag{5}$$

where the first term on the right-hand side represents the information flowing from all the X_k to X_i (including the influence of X_i on itself), and the last term is the effect of noise, computed following Liang (2021).

When $\tau_{j\rightarrow i}$ is statistically different from 0, X_j has an influence on X_i, while if $\tau_{j\rightarrow i}$ = 0 there is no influence. A value of $|\tau|$ = 100 % indicates that X_j has the maximum influence on X_i. A positive (negative) value is indicative of an increase (decrease) in variability of the target variable due to the causal influence of the source. Statistical significance of $\tau_{j\rightarrow i}$ is computed via

https://doi.org/10.5194/egusphere-2022-1340
Preprint. Discussion started: 2 December 2022

bootstrap resampling with replacement of all terms included in Eq. (3)-(5) using 500 realizations. These boostrap realizations are combined together using the False Discovery Rate (FDR) from Wilks (2016) with a significance (α) level of 5% (1% for the control simulation to take into account the effect of a larger time series). A 3-by-3 window median filter is applied to remove isolated significant points. A significant rate of information transfer from OHT convergence to OHC tendency indicates that ocean dynamics plays a role in changing OHC tendency, while a significant rate of information transfer from Qnet to OHC tendency is an indication of a thermodynamical influence.

As our ocean heat budget omits vertical mixing, which can be important in the mixed layer (Small et al., 2020), as well as horizontal mixing and sub-monthly OHT variations, we also compute a residual term in the upper 50 m as the difference between OHC tendency and the sum of OHT convergence and Qnet for the EC-Earth3-HR model simulation, in order to check its relative contribution to changes in OHC compared to OHT convergence and Qnet. We compute the rate of information transfer for five different combinations, as discussed in Sect. 3.4.

3 Results and Discussion

3.1 Upper 50 m

We first compute the rate of information transfer when considering OHT convergence and OHC tendency in the upper 50 m. Low-resolution model configurations (ocean resolution of 1°) present a significant number of regions with a strong rate of information transfer from OHT convergence to OHC tendency, in particular in the North Atlantic, North Pacific and many parts of the Southern Hemisphere (Fig. 1a for EC-Earth3-LR; Figs. A1a-A2a for other model configurations). This result suggests that variations in ocean heat content in the upper 50 m are partly dynamically driven in these specific regions at low resolution. The majority of these regions show negative values, meaning that variations in OHT convergence tend to reduce the variability in OHC tendency. Nevertheless, the number of regions with a thermodynamical influence, i.e. from Qnet to OHC tendency, is larger than the one with a dynamical influence (Fig. 1b; Figs. A1b-A2b for other model configurations). In terms of thermodynamical influence, positive rates of information transfer are present in tropical regions and near sea-ice edges, and negative values dominate in extra-tropical regions. A larger influence of air-sea fluxes on ocean heat content variations, compared to ocean dynamics, was also found by Small et al. (2020) at low resolution in the upper 50 m. It is also worth noticing that the different low-resolution model configurations broadly agree in terms of dynamical and thermodynamical influences (Figs. 1 and A1-A2).

Next, we turn to high-resolution model configurations, which feature an ocean resolution finer than, or equal to 0.25° (Table 1). We find that these models present a very small number of regions with a significant rate of information transfer from OHT convergence to OHC tendency (Fig. 2a for EC-Earth3-HR; Figs. A3a-A6a for other model configurations). This means that almost no significant dynamical influence on OHC tendency is detected at high resolution, contrarily to low resolution. On the contrary, a substantial part of the world is covered by a strong rate of information transfer from Qnet to OHC tendency (Fig. 2b; Figs. A3b-A6b for other model configurations). This highlights the large thermodynamical influence on OHC tendency at high resolution in the upper 50 m. Furthermore, the fraction of the world covered by a significant influence of Qnet

https://doi.org/10.5194/egusphere-2022-1340
Preprint. Discussion started: 2 December 2022

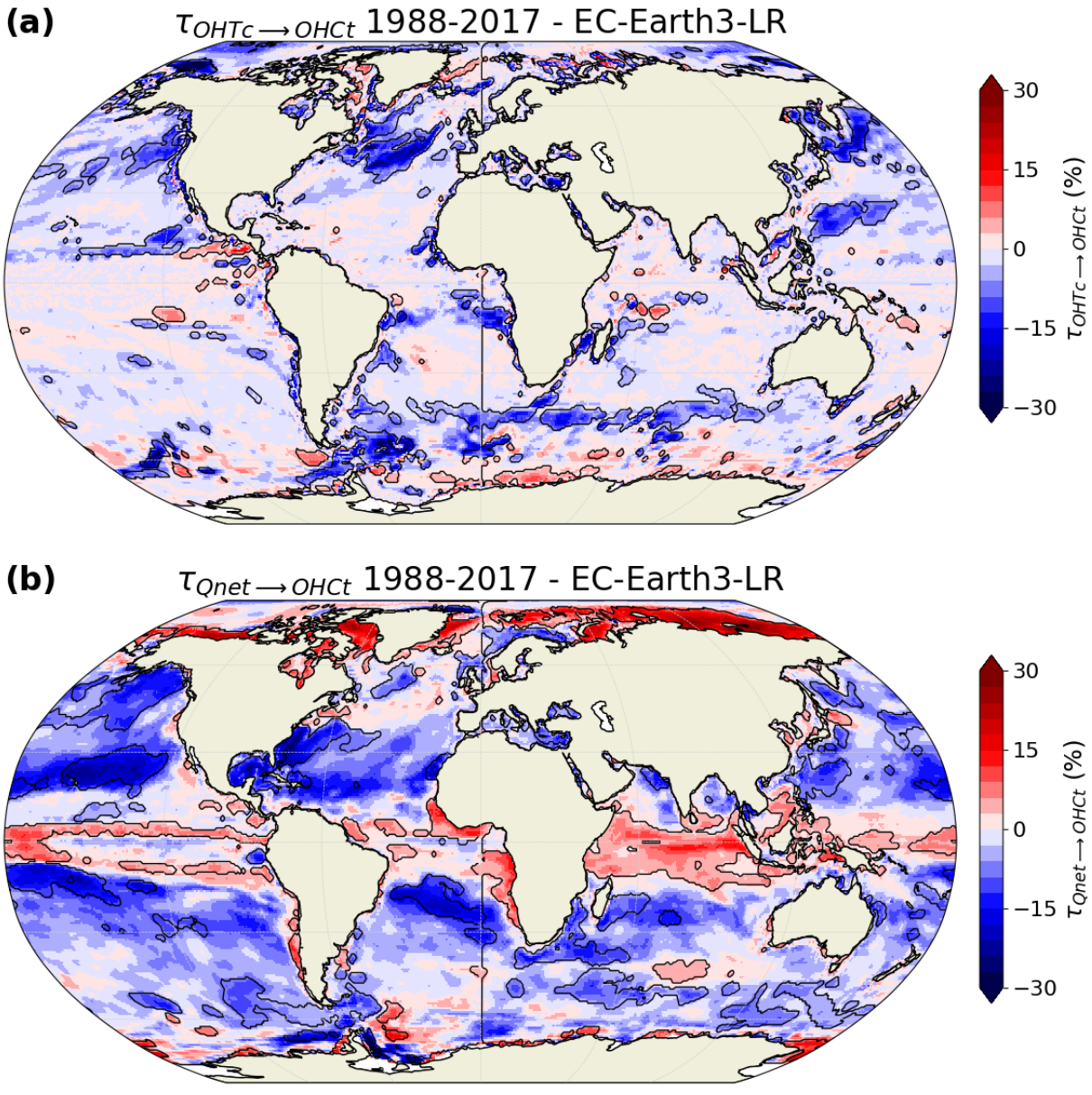

Figure 1. Relative rate of information transfer τ (a) from ocean heat transport convergence (OHTc, upper 50 m) to ocean heat content tendency (OHCt, upper 50 m) and (b) from net surface heat flux (Qnet) to OHCt, based on EC-Earth3-LR. Black contours are drawn around regions with a statistically significant transfer of information (FDR 5%; 500 bootstrap samples; median filter).

https://doi.org/10.5194/egusphere-2022-1340
Preprint. Discussion started: 2 December 2022

on OHC tendency is larger at high resolution compared to low resolution, and values are mostly positive at high resolution (changes in Qnet make OHC tendency more variable), while both positive and negative values co-exist at low resolution. As for low resolution, the different high-resolution model configurations broadly agree in terms of dynamical and thermodynamical influences (Figs. 2 and A3-A6).

The small dynamical influence and large thermodynamical contribution at high resolution is confirmed by the analysis of a 100-year control run performed with EC-Earth3-HR (Fig. A7), showing results very similar to the historical run done with the same model (Fig. 2). This result is in contradiction with Small et al. (2020), who found a larger ocean dynamical influence compared to air-sea fluxes at high resolution when considering the upper 50 m. However, several important differences exist compared to our study: Small et al. (2020) use a regression analysis and do not compute any causal relationship between variables; they include sub-monthly variations in the dynamical contribution and vertical mixing in the thermodynamical contribution; and they use a relatively short model run (8 years compared to 30 years in our study), which could explain differences between our results and theirs.

The ORAS5 reanalysis, which has an ocean resolution of 0.25°, provides rates of information transfer in agreement with high-resolution model configurations. Changes in OHC tendency are almost entirely dominated by variations in Qnet while the dynamical influence is almost absent (Fig. 3). This provides further evidence that the weak dynamical influence at high resolution (Fig. 2) is robust. It is interesting to note that the spatial distribution of the rate of information transfer from Qnet to OHC tendency at high resolution (Fig. 2b) and in ORAS5 (Fig. 3b) shares many similarities with the one from turbulent heat flux to SST tendency using satellite observations over the same time period (Fig. 3b in Docquier et al. 2022a). Turbulent heat flux and SST tendency can be seen as proxies of net surface heat flux (Qnet) and OHC tendency in the upper ocean, respectively. This agreement with our analysis of observations provides additional confidence in the results found at high resolution.

Low-resolution model configurations have a lower skill in terms of representing ocean currents and the mean climate (Kirtman et al., 2012; Grist et al., 2018; Docquier et al., 2019). Combined with the large difference in terms of rate of information transfer between low (Fig. 1a) and high (Fig. 2a) resolutions, we suggest that low-resolution model configurations overestimate the dynamical influence of the ocean in driving changes in OHC tendency. Instead, the thermodynamical influence, as represented by high-resolution model configurations, appears to strongly control variations in ocean heat content in the upper 50 m of the ocean (Fig. 2b). To further demonstrate that the difference in the rate of information transfer between low and high resolutions is robust, we have upscaled ocean velocity (meridional and zonal components) and potential temperature as well as the atmospheric heat flux terms of EC-Earth3-HR to the same resolution as EC-Earth3-LR (i.e. 100 km in both the ocean and atmosphere). We have then re-computed OHC tendency, OHT convergence and Qnet, and subsequently the rate of information transfer, based on the upscaled quantities. Results are presented in Fig. A8 and are mostly similar to the rate of information transfer computed with EC-Earth3-HR without upscaling (Fig. 2), showing a weak ocean dynamical influence. Upscaling to 400 km provides similar results (not shown). This confirms that the results found strongly depend on the model resolution and its related processes, and not on length scale.

https://doi.org/10.5194/egusphere-2022-1340
Preprint. Discussion started: 2 December 2022

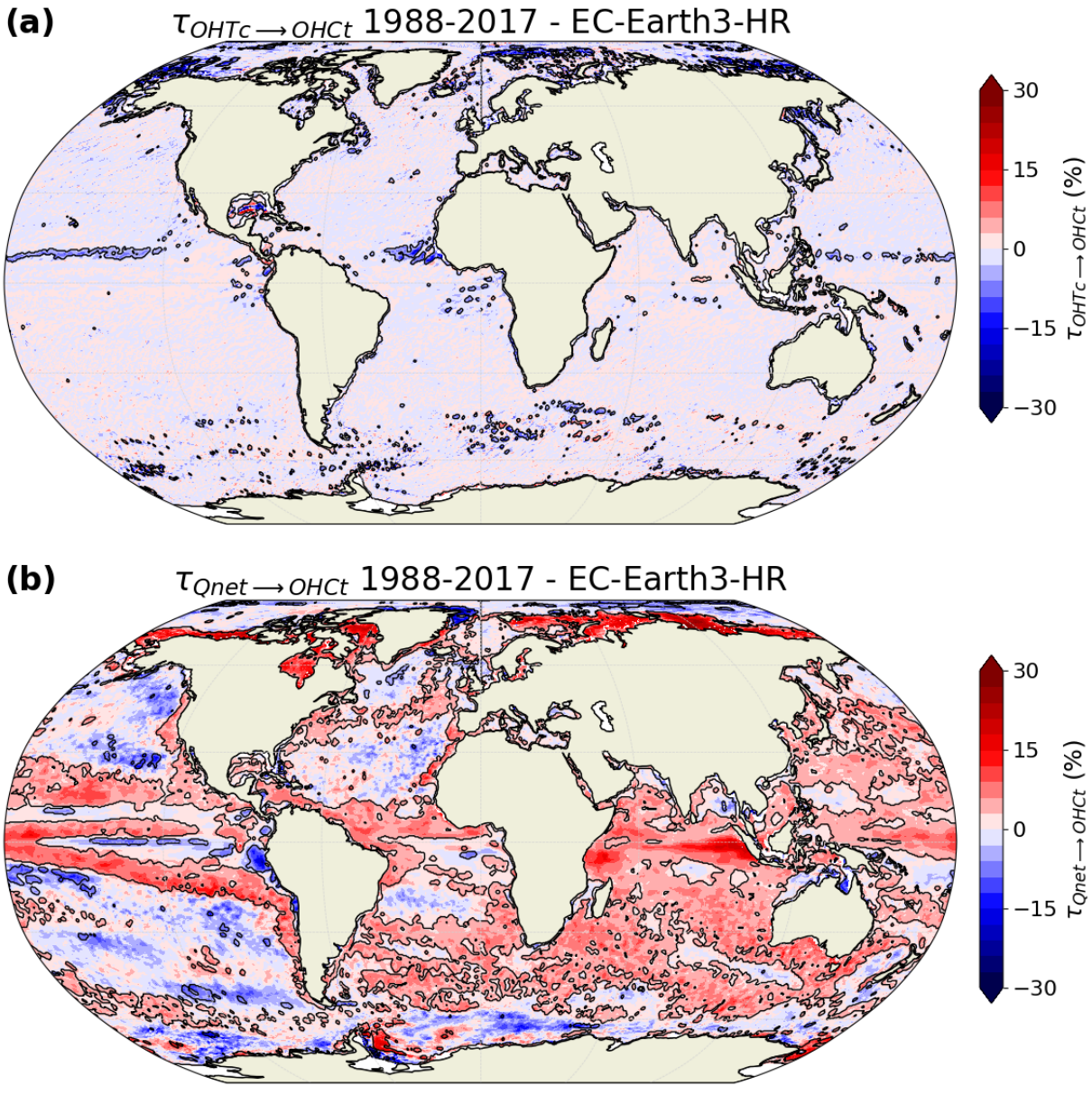

Figure 2. Relative rate of information transfer τ (a) from ocean heat transport convergence (OHTc, upper 50 m) to ocean heat content tendency (OHCt, upper 50 m) and (b) from net surface heat flux (Qnet) to OHCt, based on EC-Earth3-HR. Black contours are drawn around regions with a statistically significant transfer of information (FDR 5%; 500 bootstrap samples; median filter).

https://doi.org/10.5194/egusphere-2022-1340
Preprint. Discussion started: 2 December 2022

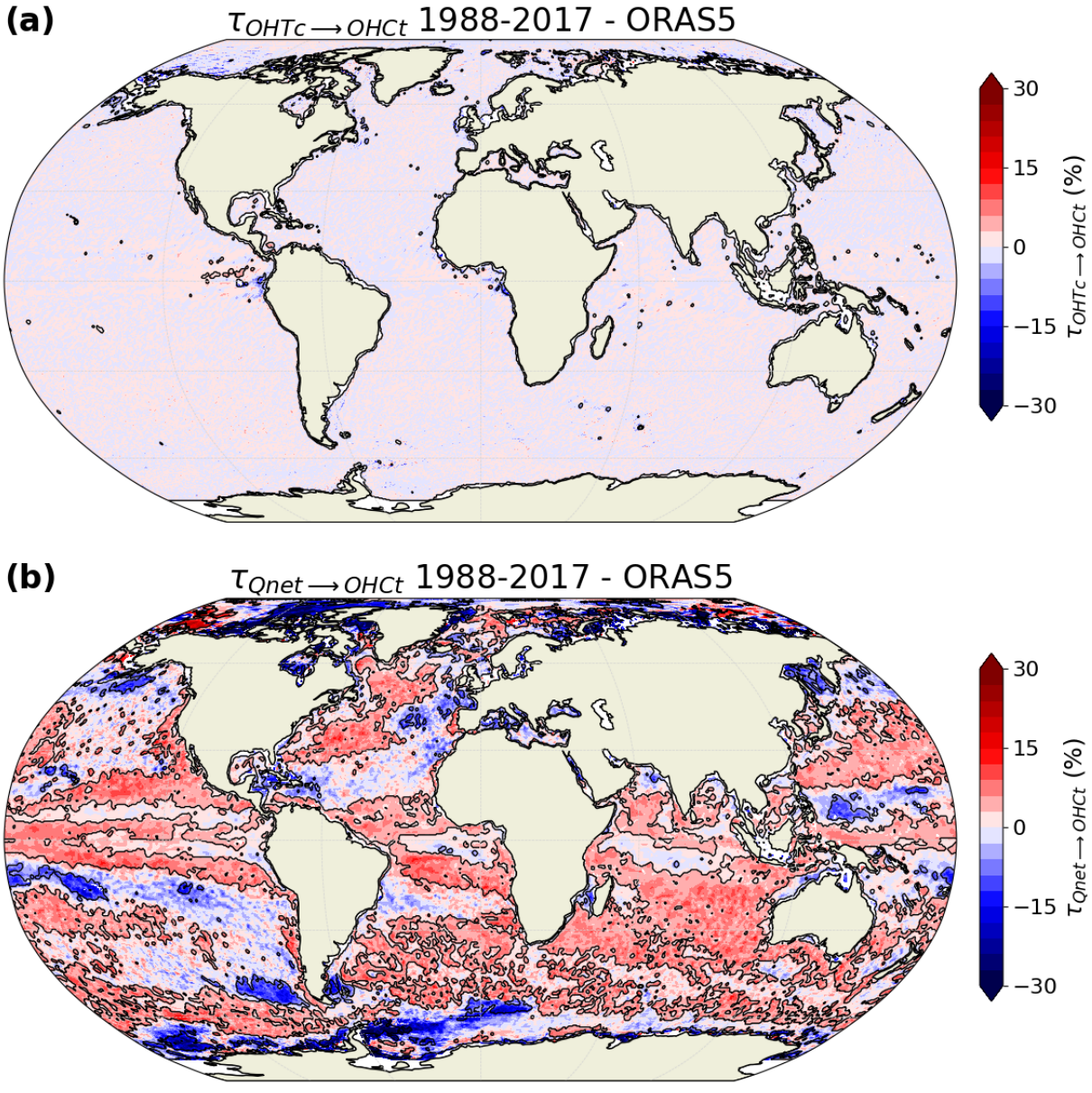

Figure 3. Relative rate of information transfer τ (a) from ocean heat transport convergence (OHTc, upper 50 m) to ocean heat content tendency (OHCt, upper 50 m) and (b) from net surface heat flux (Qnet) to OHCt, based on ORAS5. Black contours are drawn around regions with a statistically significant transfer of information (FDR 5%; 500 bootstrap samples; median filter).

https://doi.org/10.5194/egusphere-2022-1340
Preprint. Discussion started: 2 December 2022

3.2 Upper 300 m

We then consider OHC tendency and OHT convergence in the upper 300 m and re-compute the rate of information transfer. In this case, a larger number of regions with a significant influence of OHT convergence on OHC tendency is found compared to the upper 50 m. On the contrary, the number of regions with a significant influence of Qnet on OHC tendency in the upper 300 m becomes smaller relative to the upper 50 m. This is true for both low (Fig. 4) and high (Fig. 5) resolutions, as well as ORAS5 (Fig. 6). This suggests an increase of the dynamical contribution with a deeper integration of OHC and OHT. This result is in agreement with Small et al. (2020), who use CCSM4 at low (1°) and high (0.1°) ocean resolutions. However, the relative importance of ocean dynamics is smaller in our study compared to the latter study. This could be due to the different methodology and/or the much shorter considered time period in Small et al. (2020), as already mentioned in Sect. 3.1.

At low resolution, the number of regions with a significant influence of ocean dynamics on OHC tendency becomes larger than the influence of air-sea heat fluxes (Fig. 4) compared to the upper 50 m (Fig. 1). This is in agreement with results found in Small et al. (2020) for the upper 400 m and Roberts et al. (2017) for the mixed layer. At high resolution, despite the increase in the number of regions with a significant ocean dynamics influence in the upper 300 m compared to the upper 50 m, the thermodynamical influence still dominates (Fig. 5). This is confirmed by results from the reanalysis, for which the number of regions with a significant dynamical influence remains limited (Fig. 6). Note that in certain regions, differences are present between the reanalysis and EC-Earth3-HR in terms of the thermodynamical influence on OHC tendency. For example, an extensive region of positive rate of information transfer is present in the North Atlantic subpolar gyre in ORAS5 (Fig. 6b), while there is a relatively small zone of negative information transfer in EC-Earth3-HR (Fig. 5b).

Despite the increase of the dynamical contribution and decrease of the thermodynamical influence from 50 m to 300 m, the spatial distribution of these influences remains relatively similar for both depth integrations. At low resolution, negative values of the dynamical influence dominate in many regions of the world (Figs. 1a and 4a). This means that variations in OHT convergence tend to stabilize OHC tendency. Also, at low resolution, the thermodynamical contribution has positive values of the rate of information transfer in most of the tropics and in polar regions (Figs. 1b and 4b), suggesting that the Qnet variability tends to increase the OHC tendency variability in these regions. On the contrary, negative values of the thermodynamical influence are present in most extratropical regions. At high resolution, even if the dynamical contribution remains limited, we can see a dominance of negative values of information transfer (Figs. 2a and 5a), similarly to low resolution. Contrarily to low resolution, mostly positive values of the thermodynamical influence are modeled at high resolution (Figs. 2b and 5b).

3.3 Difference between low and high resolutions

The presence of a stronger signal in the dynamical influence, as measured by the rate of information transfer from OHT convergence to OHC tendency, at low resolution compared to high resolution is partly due to a much smoother spatial distribution of ocean velocity field at low resolution (Fig. 7a). This results in a relatively smooth spatial distribution of OHT convergence at low resolution. At high resolution, the ocean velocity field is highly variable in space (Fig. 7b), resulting in a much noisier OHT convergence spatial variability. Note that in Fig. 7b, the ocean velocity is interpolated onto the low-resolution grid to be

https://doi.org/10.5194/egusphere-2022-1340
Preprint. Discussion started: 2 December 2022

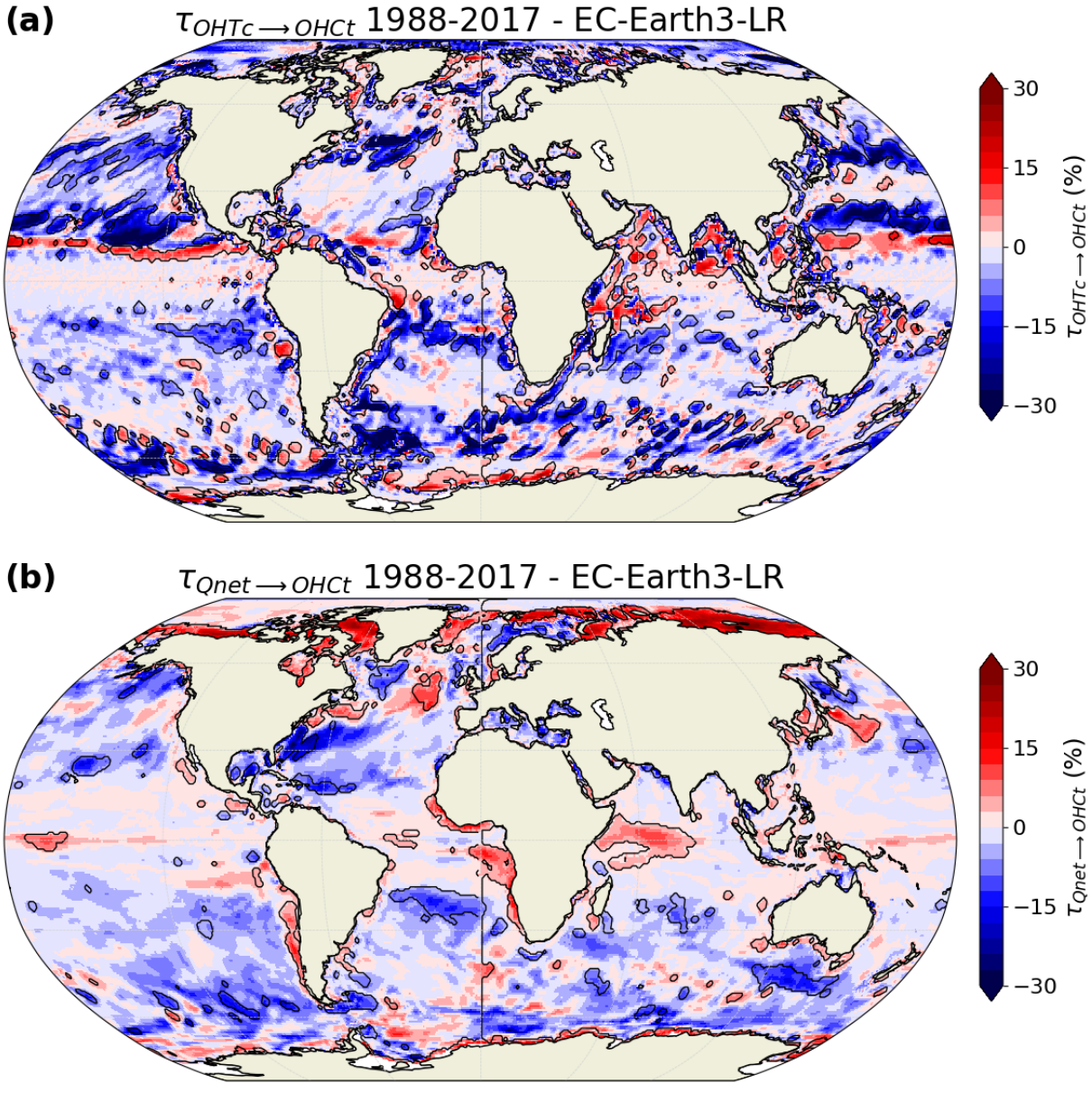

Figure 4. Relative rate of information transfer τ (a) from ocean heat transport convergence (OHTc, upper 300 m) to ocean heat content tendency (OHCt, upper 300 m) and (b) from net surface heat flux (Qnet) to OHCt, based on EC-Earth3-LR. Black contours are drawn around regions with a statistically significant transfer of information (FDR 5%; 500 bootstrap samples; median filter).

https://doi.org/10.5194/egusphere-2022-1340
Preprint. Discussion started: 2 December 2022

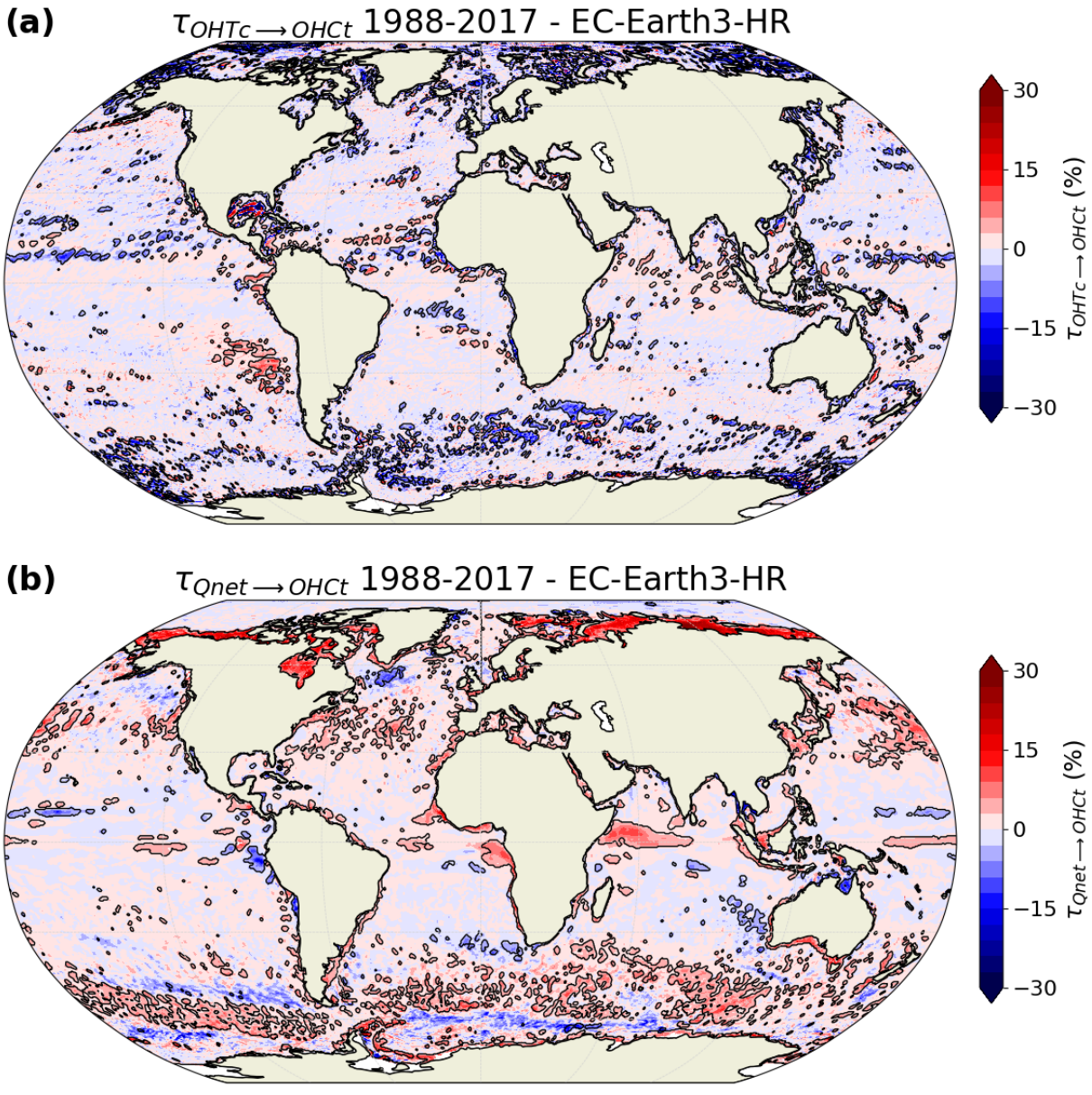

Figure 5. Relative rate of information transfer τ (a) from ocean heat transport convergence (OHTc, upper 300 m) to ocean heat content tendency (OHCt, upper 300 m) and (b) from net surface heat flux (Qnet) to OHCt, based on EC-Earth3-HR. Black contours are drawn around regions with a statistically significant transfer of information (FDR 5%; 500 bootstrap samples; median filter).

https://doi.org/10.5194/egusphere-2022-1340
Preprint. Discussion started: 2 December 2022

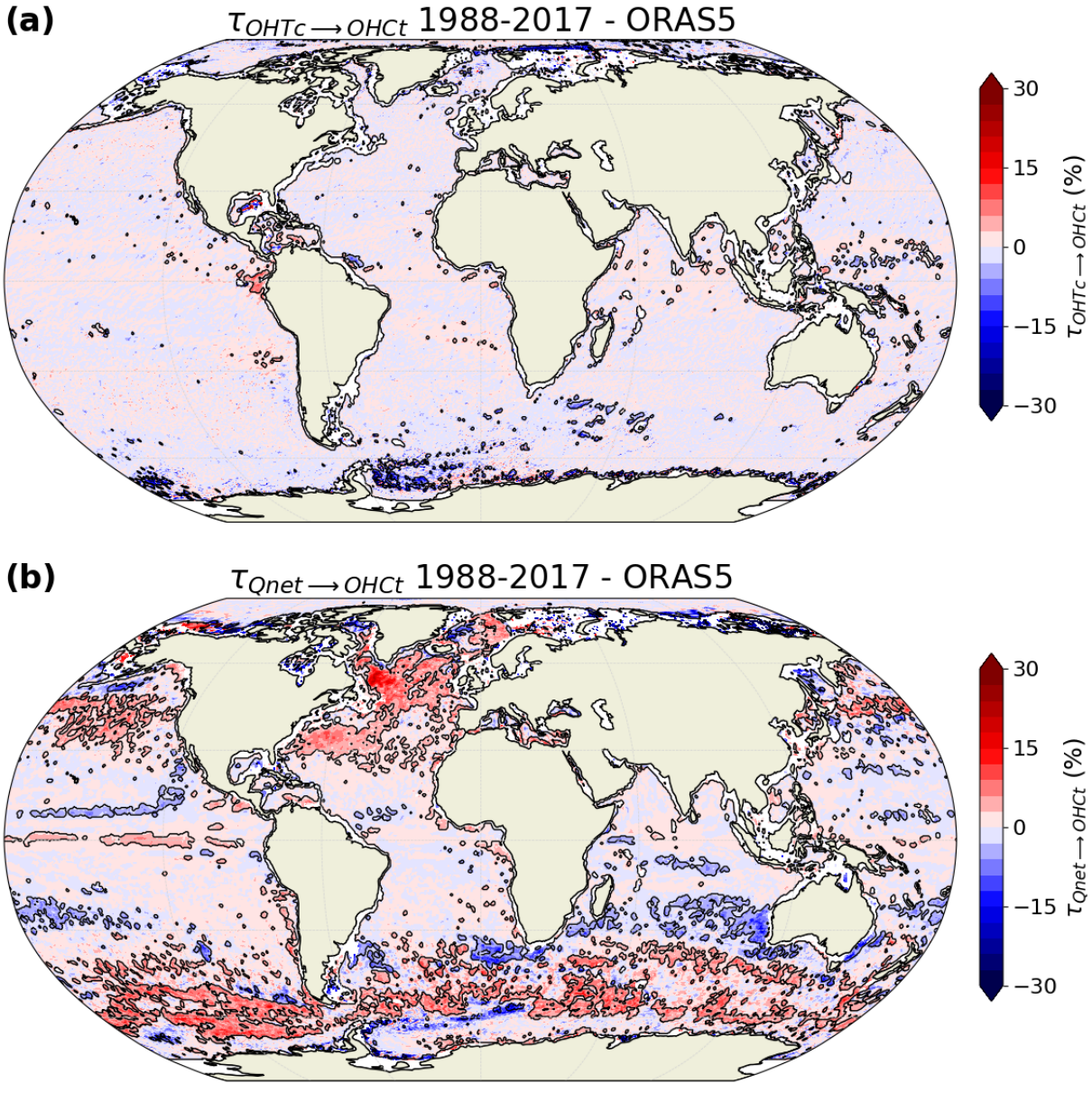

Figure 6. Relative rate of information transfer τ (a) from ocean heat transport convergence (OHTc, upper 300 m) to ocean heat content tendency (OHCt, upper 300 m) and (b) from net surface heat flux (Qnet) to OHCt, based on ORAS5. Black contours are drawn around regions with a statistically significant transfer of information (FDR 5%; 500 bootstrap samples; median filter).

https://doi.org/10.5194/egusphere-2022-1340
Preprint. Discussion started: 2 December 2022

comparable to Fig. 7a. Despite this spatial interpolation, the velocity field is still much noisier at high resolution compared to low resolution.

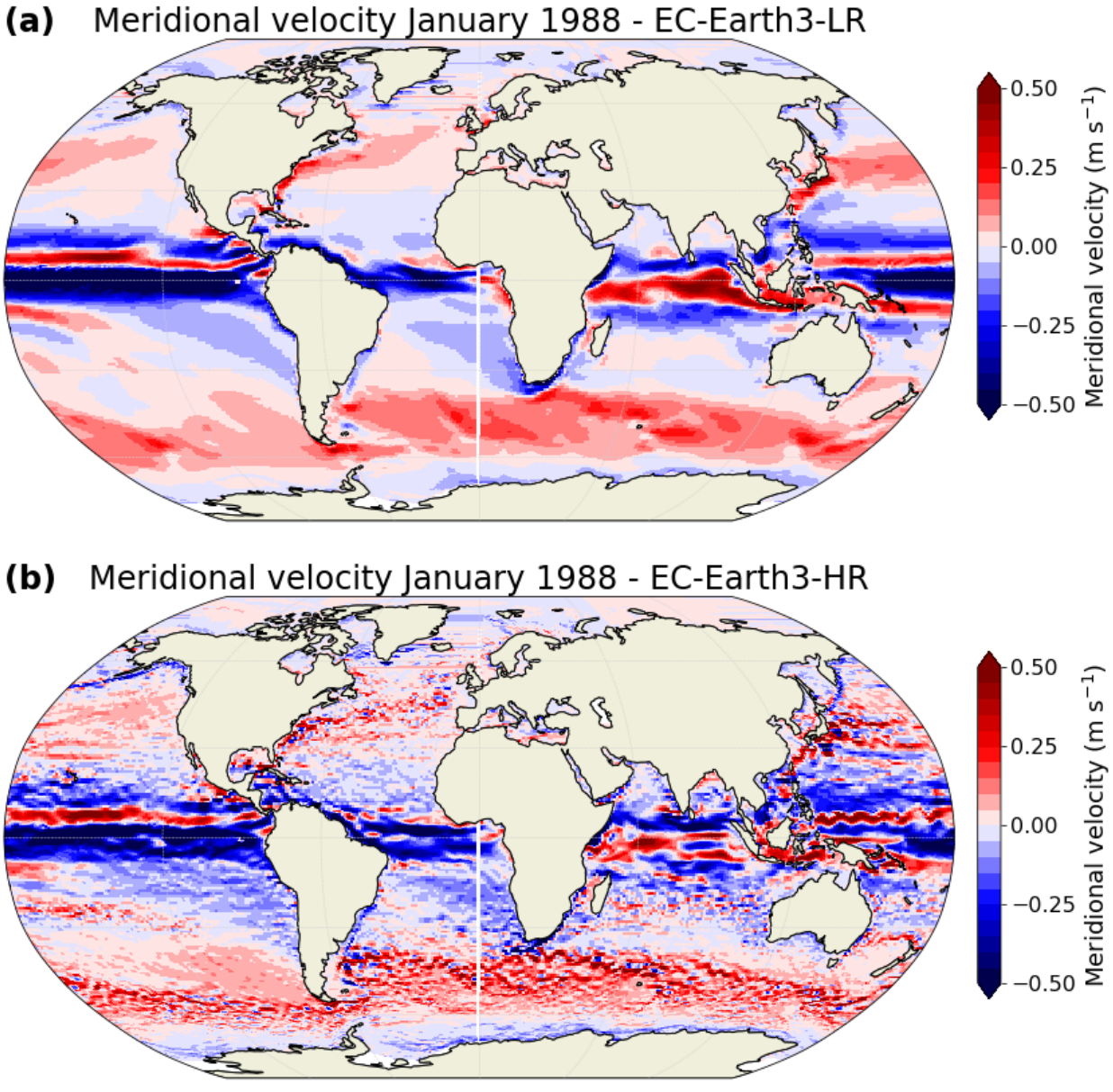

Figure 7. Ocean surface meridional velocity in January 1988 for (a) EC-Earth3-LR and (b) EC-Earth3-HR (the latter is interpolated onto the EC-Earth3-LR grid).

https://doi.org/10.5194/egusphere-2022-1340
Preprint. Discussion started: 2 December 2022

This difference in spatial smoothness of the velocity field at both resolutions results in large discrepancies in terms of correlation and causal influence between OHT convergence and OHC tendency. The two fields are correlated in a much larger number of regions at low resolution compared to high resolution (Fig. 8). At high resolution, a significant number of regions, notably in the North Atlantic and Southern Hemisphere, present no correlation (Fig. 8b). This affects the rate of information transfer from OHT convergence to OHC tendency as it is tightly linked to the correlation between the two variables by definition (Liang, 2014). As a result, a much larger causal influence from OHT convergence to OHC tendency is found at low resolution (Fig. 1a) compared to high resolution (Fig. 2a). This is partly due to the high spatial variability of the velocity field at high resolution.

3.4 Inclusion of residual processes

As described in Sect. 2.2, our approach does not take into account vertical mixing, which can be important in the upper ocean, as well as other processes that could affect changes in OHC. Adding a residual to the multivariate estimates results in singularities reflecting that the residual is a linear combination of the three other terms. Thus, we compute the rate of information transfer taking into account a residual term in five different combinations with the EC-Earth3-HR historical simulation.

When we combine OHC tendency, OHT convergence and the residual (thus omitting Qnet), we obtain very large influences of both OHT convergence and the residual on OHC tendency, especially in tropical regions and western boundary currents, albeit with opposite signs (Fig. A9). However, this combination omits an important driver, which is the air-sea heat flux (Qnet), so the rates of information transfer are biased due to this absence. If we repeat the procedure with OHC tendency, Qnet and the residual (omitting OHT convergence), the thermodynamical influence (Fig. A10a) stays very similar to the original case with OHC tendency, OHT convergence and Qnet (Fig. 2b). Also, the residual influence on OHC tendency (Fig. A10b) is relatively similar to the dynamical influence in the original case (Fig. 2a).

The three next combinations only involve two variables at a time (which we refer to as 2D), i.e. OHT convergence and OHC tendency, Qnet and OHC tendency, and the residual and OHC tendency. Results are summarized in Fig. 9 and reveal that the 2D dynamical (Fig. 9a) and thermodynamical (Fig. 9b) influences on OHC tendency are very similar to the original three-variable (3D) case (Fig. 2). The residual influence (Fig. 9c) stays very similar to the dynamical influence (Fig. 9a) in the 2D case, in a similar way as the original 3D case (Fig. A10b). This suggests that the results found in the 3D case are robust, i.e. the variations of OHC are largely dominated by changes in Qnet.

3.5 Limitations of the method

The causal method used in our study has several strong advantages, including its derivation from first principles of information entropy (Liang, 2016), the possibility to identify the direction and magnitude of causal influences between variables, and its relative simplicity (see Eq. 3). However, several limitations exist.

The first limitation is that the method has been designed for linear systems (Liang, 2014). While it has been tested and validated with highly nonlinear examples (Liang, 2014), we should keep in mind that the approach provides an approximated solution, and a generalization to the fully nonlinear case should be developed to get a more accurate solution (Liang, 2021).

https://doi.org/10.5194/egusphere-2022-1340
Preprint. Discussion started: 2 December 2022

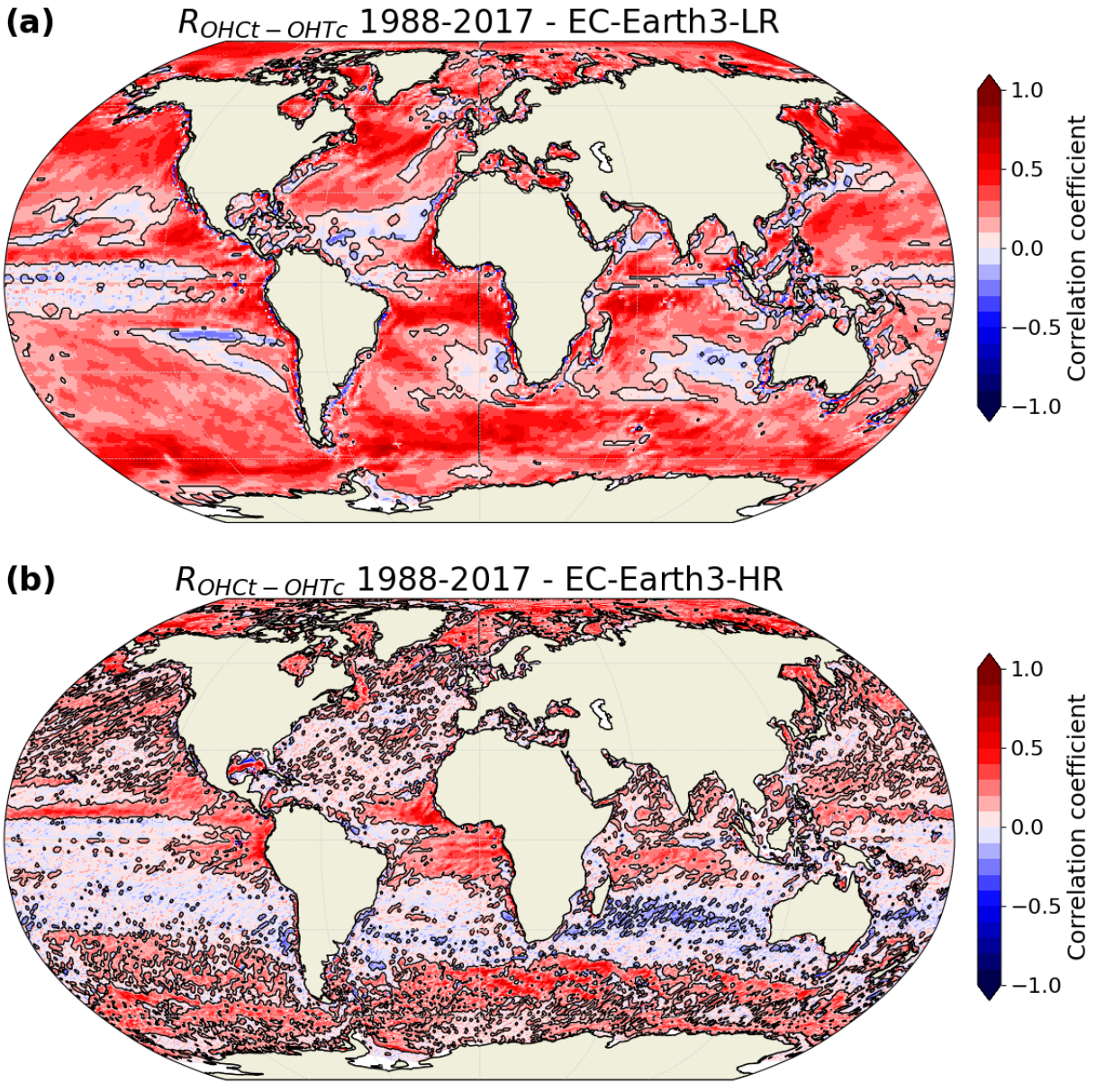

Figure 8. Pearson correlation coefficient between ocean heat content tendency (OHCt, upper 50 m) and ocean heat transport convergence (OHTc, upper 50 m), based on (a) EC-Earth3-LR and (b) EC-Earth3-HR. Black contours are drawn around regions with a statistically significant correlation coefficient (FDR 5%; Student's t-test; median filter).

https://doi.org/10.5194/egusphere-2022-1340
Preprint. Discussion started: 2 December 2022

The second limitation is the problem of hidden variables and is linked to the tests we have done in Sect. 3.4 with the residual. When we omit Qnet in the computation of the rate of information transfer, we end up with large but opposite influences of OHT convergence and the residual on OHC tendency (Fig. A9). This is unrealistic, as revealed by the original case (Fig. 2). Thus, careful attention needs to be taken in choosing the right variables for specific studies. Since the lack of an important driver may lead to unrealistic results, verifying the robustness of the results of the 3D analysis with 2D analyses (as done in Sect. 3.4) should prevent misinterpretation in cases where this driver could not be identified or taken into account.

Finally, despite the success of this method in different studies, including climate analyses (Sect. 1), no detailed study has compared the rate of information transfer to other causal methods yet. Such an intercomparison with a dedicated benchmark would provide more insights into the pros and cons of the method developed by Liang and Kleeman (2005).

4 Conclusions

In our study, we have applied the rate of information transfer developed by Liang and Kleeman (2005) and recently extended to multivariate cases (Liang, 2021) to the study of the ocean heat budget over 1988-2017. More precisely, we have quantified the relative contributions from OHT convergence (dynamical influence) and Qnet (thermodynamical influence) in driving changes in OHC, using two different depth integrations (50 m and 300 m). We have used three different coupled global climate models with at least two different configurations and have investigated the role of ocean resolution. The use of the ORAS5 reanalysis has allowed us to confirm the robustness of our results.

We have found that when integrated over the upper 50 m, OHC tendency is clearly dominated by thermodynamical changes (Qnet) at high ocean resolution ($\leq 0.25°$), while both dynamical and thermodynamical influences are at play at low ocean resolution (1°). When taking into account the upper 300 m, the number of regions with a dynamical influence increases: it becomes comparable to the thermodynamical influence at high resolution and becomes even larger at low resolution. The very small dynamical influence in the upper 50 m at high resolution is not in agreement with Small et al. (2020), which could be due to the differences in the method used (regression analysis), the model configuration and the much shorter period used in Small et al. (2020).

We have identified that one of the reasons for the large difference between low and high resolutions in terms of dynamical influence is related to the spatial variability of the ocean velocity field. At low resolution, the velocity field is relatively smooth, while it is highly variable at high resolution, which results in a smaller correlation between OHT convergence and OHC tendency at high resolution, and thus a smaller causal influence between these two variables.

Several lines of evidence demonstrate the robustness of our results. They include upscaling high-resolution variables to the low-resolution grid, using a longer control simulation and including residual processes. Upscaling ocean and atmosphere variables from high to low resolution and re-computing the rate of information transfer provides very similar results to the original high-resolution case; thus, our results are not due to the length scale, but rather to the different resolution used in models. The use of a 100-year control simulation also provides very similar results to the original case. The inclusion of a residual term, which incorporates processes not captured by OHT convergence and Qnet as computed in our study, and

https://doi.org/10.5194/egusphere-2022-1340
Preprint. Discussion started: 2 December 2022

different combinations of variables in the computation of the rate of information transfer confirms that the thermodynamical influence is the largest at high resolution in the upper 50 m.

Overall, these results suggest that low-resolution model configurations (1°) overestimate the influence of ocean dynamics on variation in ocean heat content at both depth integrations used in this study. Additional analyses, which go beyond the scope of this study, could include the close inspection of specific regions (such as western boundary currents and the North Atlantic) together with a detailed comparison with available observations.

Code and data availability. ORAS5 reanalysis data (Zuo et al., 2019) were retrieved from the portal of the Center for Earth System Research and Sustainability (CEN) from the University of Hamburg (https://www.cen.uni-hamburg.de/icdc/data/ocean/easy-init-ocean/ecmwf-oras5.html). Model data are available on the Earth System Grid Federation (ESGF) nodes (https://esgf-node.llnl.gov/search/cmip6) and references of the different datasets are provided in Table 1. The Python scripts to produce the outputs and figures of this article are available on Zenodo: https://zenodo.org/record/7358097 (Docquier, 2022).

Appendix A: Supplementary figures

https://doi.org/10.5194/egusphere-2022-1340
Preprint. Discussion started: 2 December 2022

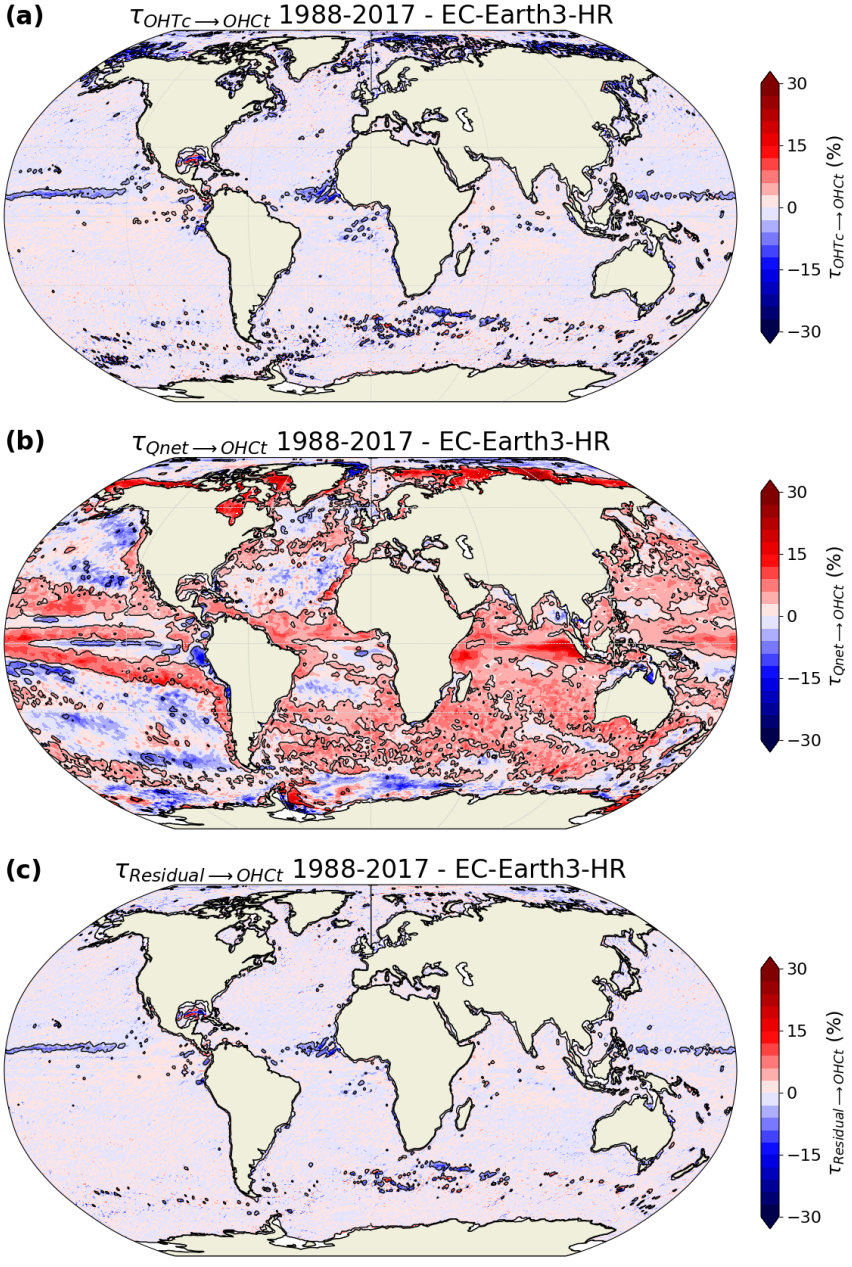

Figure 9. Relative rate of information transfer τ (a) from ocean heat transport convergence (OHTc, upper 50 m) to ocean heat content tendency (OHCt, upper 50 m) in 2D, (b) from net surface heat flux (Qnet) to OHCt in 2D, and (c) from the residual to OHCt in 2D, based on EC-Earth3-HR. Black contours are drawn around regions with a statistically significant transfer of information (FDR 5%; 500 bootstrap samples; median filter).

https://doi.org/10.5194/egusphere-2022-1340
Preprint. Discussion started: 2 December 2022

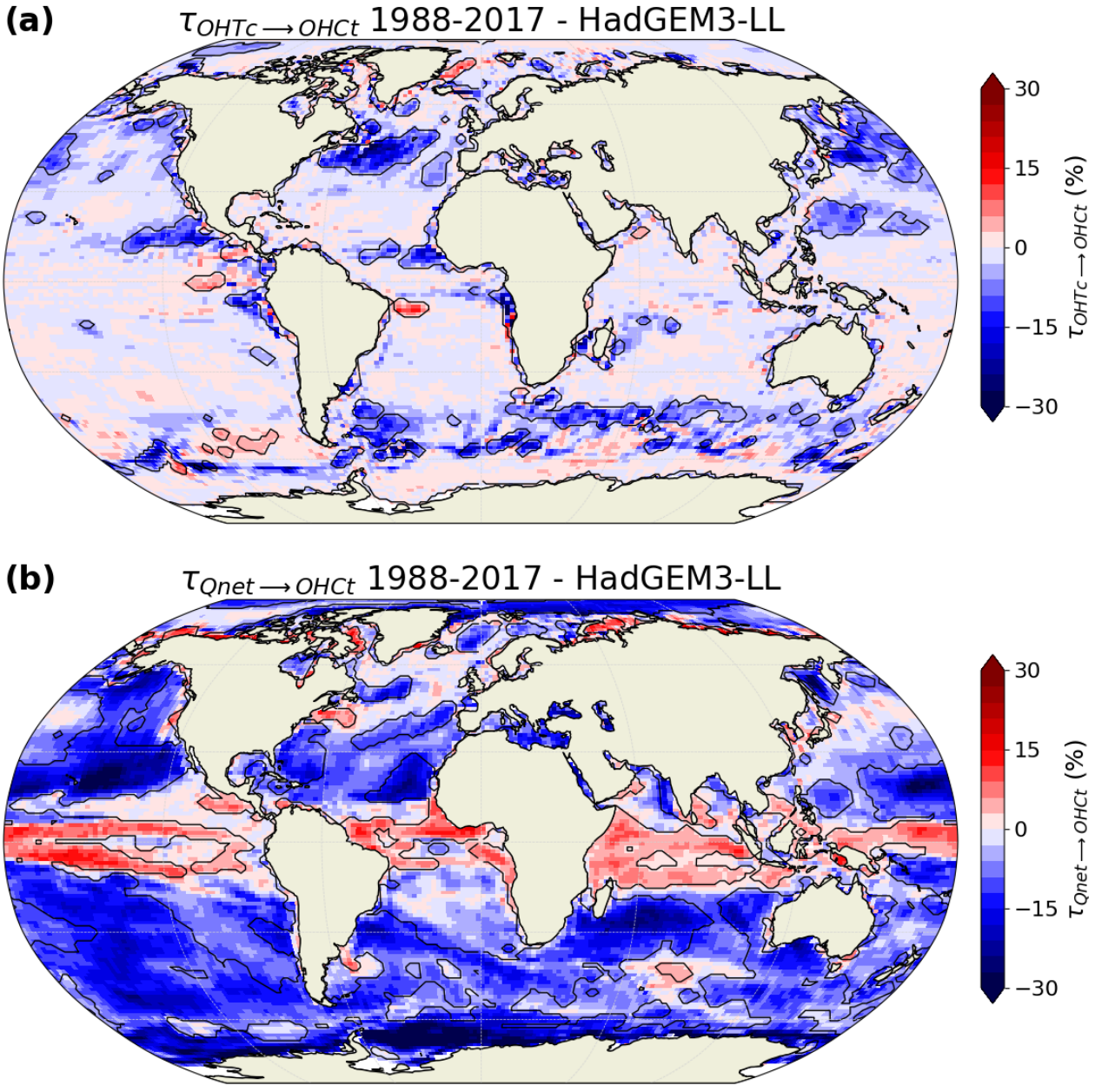

Figure A1. Relative rate of information transfer τ (a) from ocean heat transport convergence (OHTc, upper 50 m) to ocean heat content tendency (OHCt, upper 50 m) and (b) from net surface heat flux (Qnet) to OHCt, based on HadGEM3-LL. Black contours are drawn around regions with a statistically significant transfer of information (FDR 5%; 500 bootstrap samples; median filter).

https://doi.org/10.5194/egusphere-2022-1340
Preprint. Discussion started: 2 December 2022

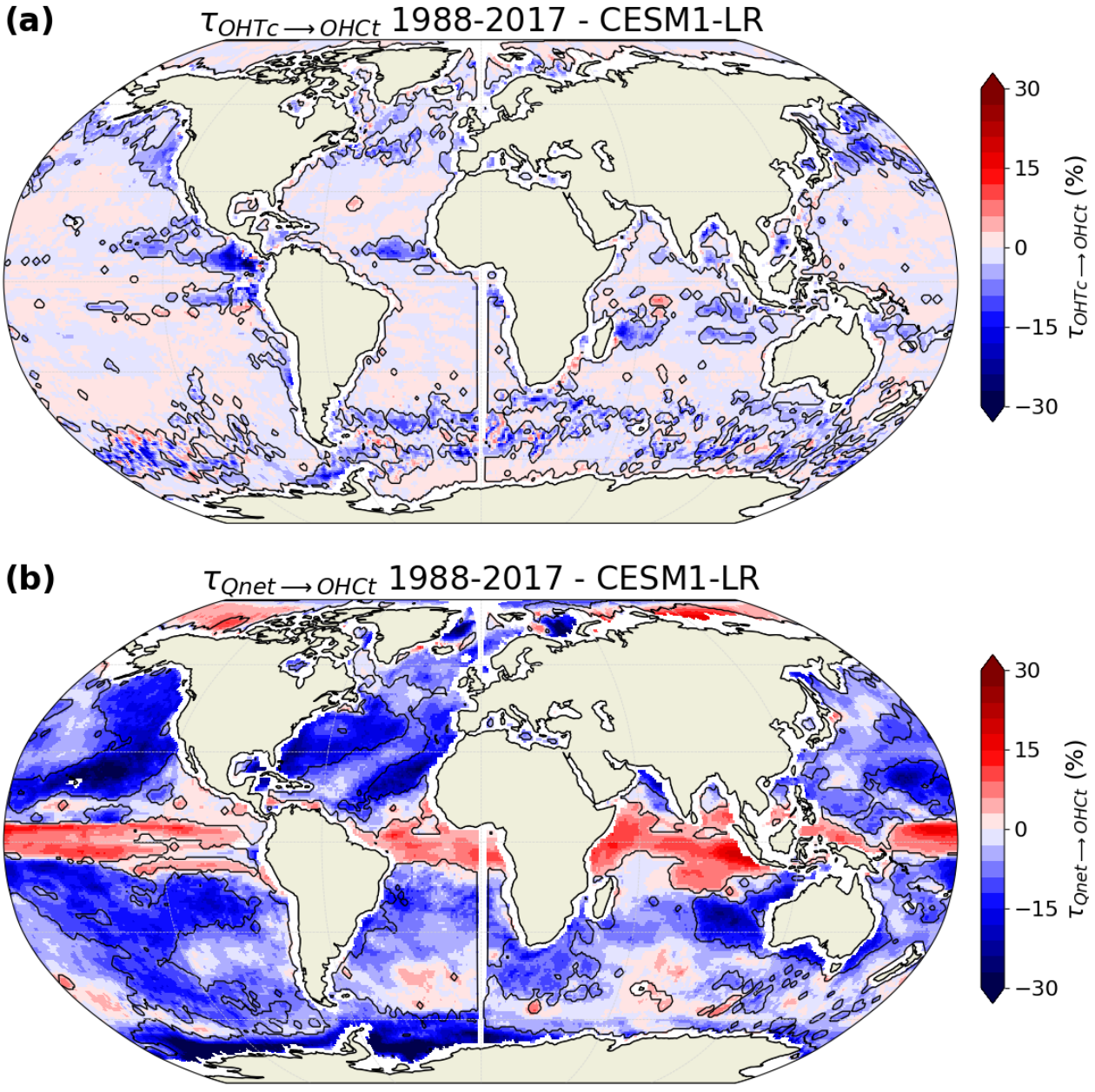

Figure A2. Relative rate of information transfer τ (a) from ocean heat transport convergence (OHTc, upper 50 m) to ocean heat content tendency (OHCt, upper 50 m) and (b) from net surface heat flux (Qnet) to OHCt, based on CESM1-LR. Black contours are drawn around regions with a statistically significant transfer of information (FDR 5%; 500 bootstrap samples; median filter).

https://doi.org/10.5194/egusphere-2022-1340
Preprint. Discussion started: 2 December 2022

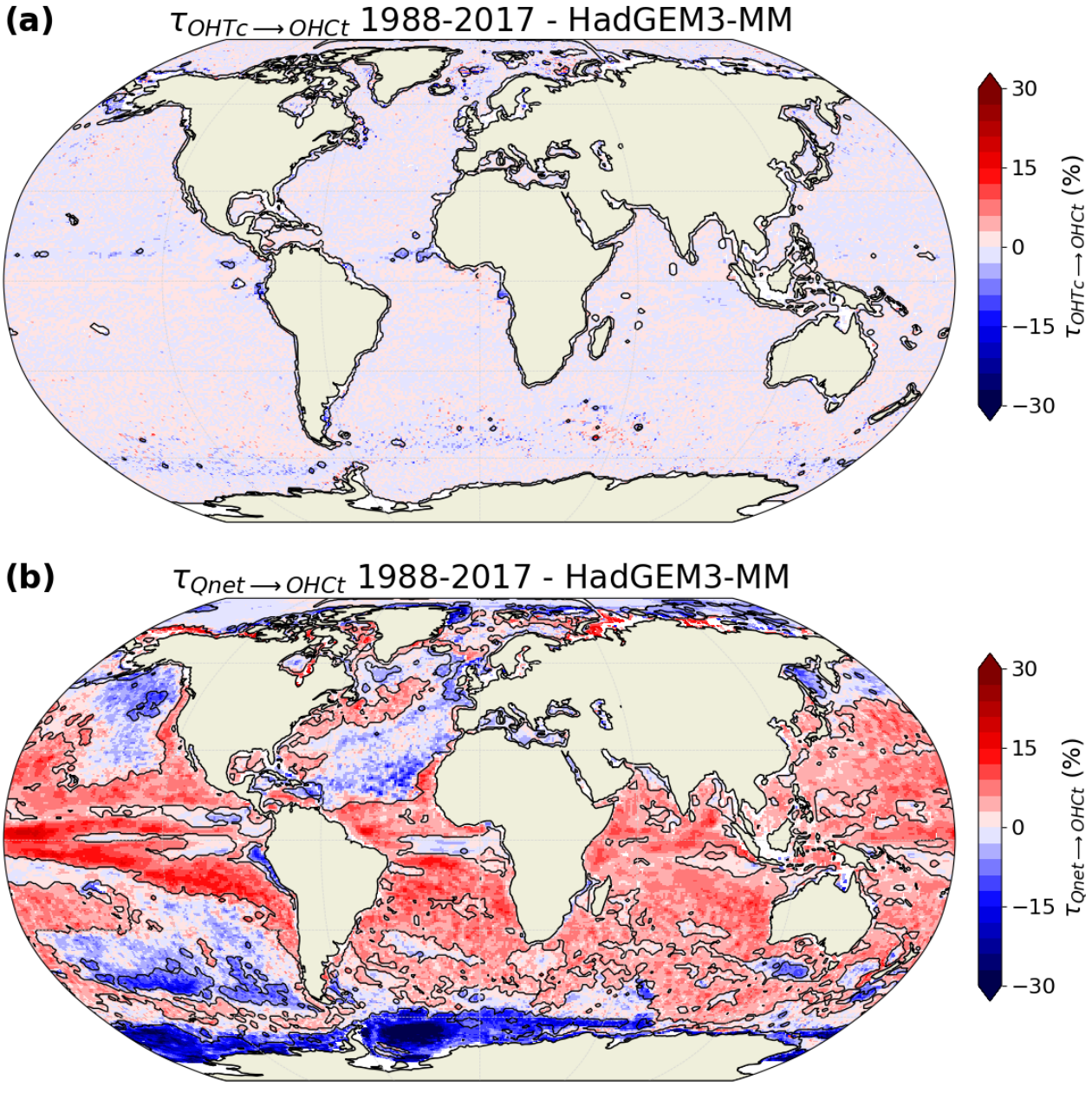

Figure A3. Relative rate of information transfer τ (a) from ocean heat transport convergence (OHTc, upper 50 m) to ocean heat content tendency (OHCt, upper 50 m) and (b) from net surface heat flux (Qnet) to OHCt, based on HadGEM3-MM. Black contours are drawn around regions with a statistically significant transfer of information (FDR 5%; 500 bootstrap samples; median filter).

https://doi.org/10.5194/egusphere-2022-1340
Preprint. Discussion started: 2 December 2022

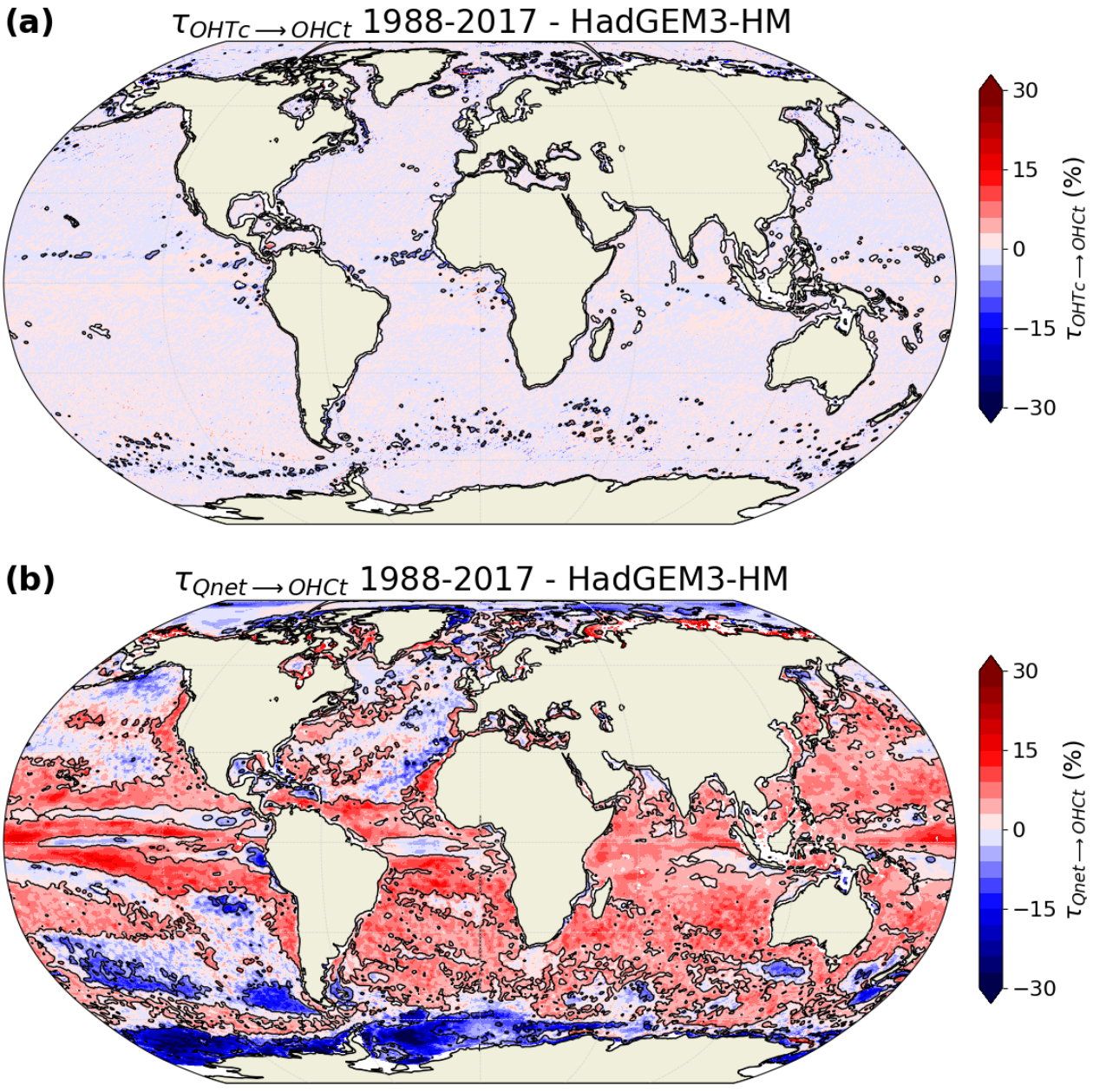

Figure A4. Relative rate of information transfer τ (a) from ocean heat transport convergence (OHTc, upper 50 m) to ocean heat content tendency (OHCt, upper 50 m) and (b) from net surface heat flux (Qnet) to OHCt, based on HadGEM3-HM. Black contours are drawn around regions with a statistically significant transfer of information (FDR 5%; 500 bootstrap samples; median filter).

https://doi.org/10.5194/egusphere-2022-1340
Preprint. Discussion started: 2 December 2022

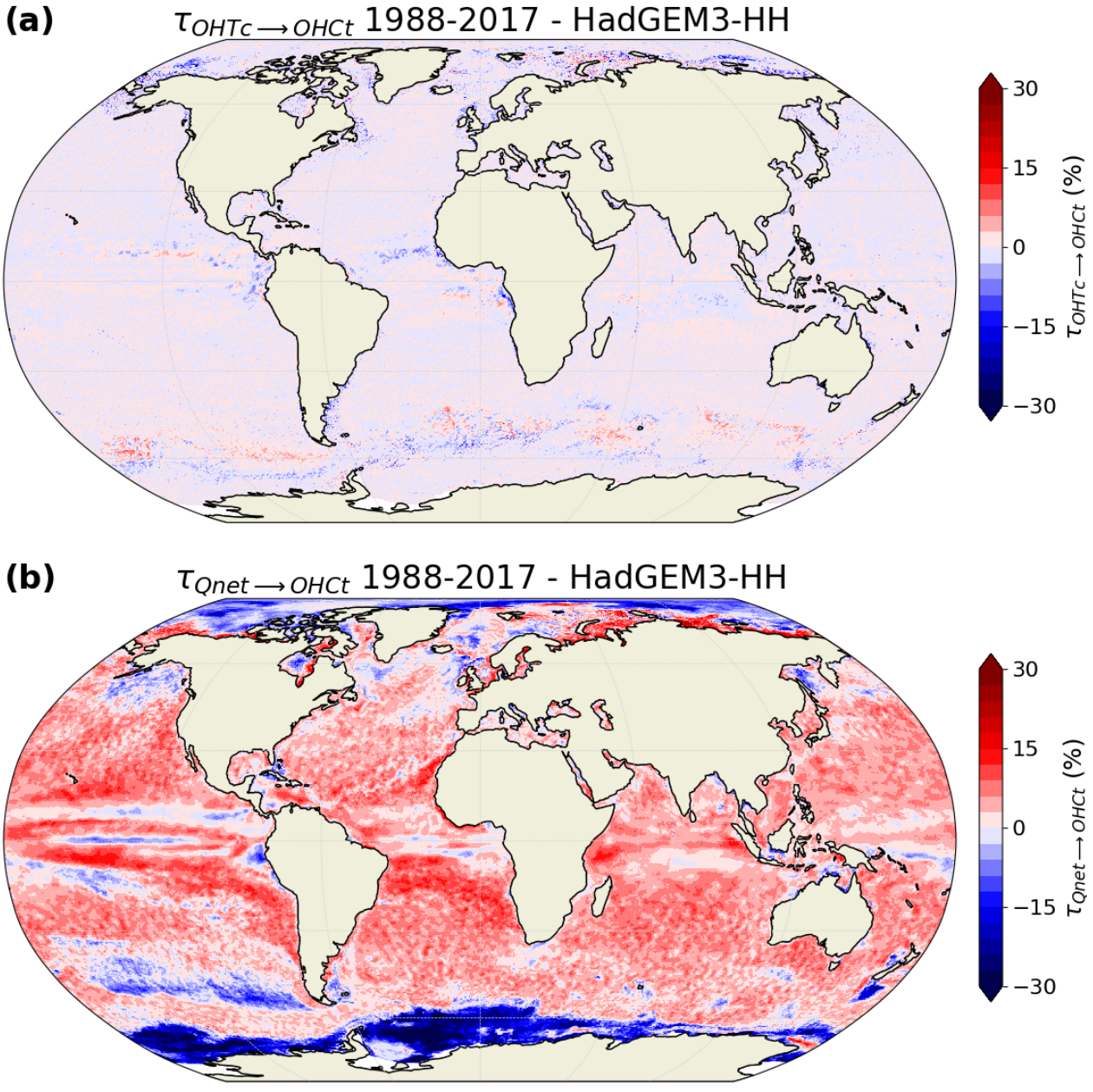

Figure A5. Relative rate of information transfer τ (a) from ocean heat transport convergence (OHTc, upper 50 m) to ocean heat content tendency (OHCt, upper 50 m) and (b) from net surface heat flux (Qnet) to OHCt, based on HadGEM3-HH. No bootstrapping has been performed for this model simulation, but results are qualitatively similar to HadGEM3-MM (Fig. A3) and HadGEM3-HM (Fig. A4).

https://doi.org/10.5194/egusphere-2022-1340
Preprint. Discussion started: 2 December 2022

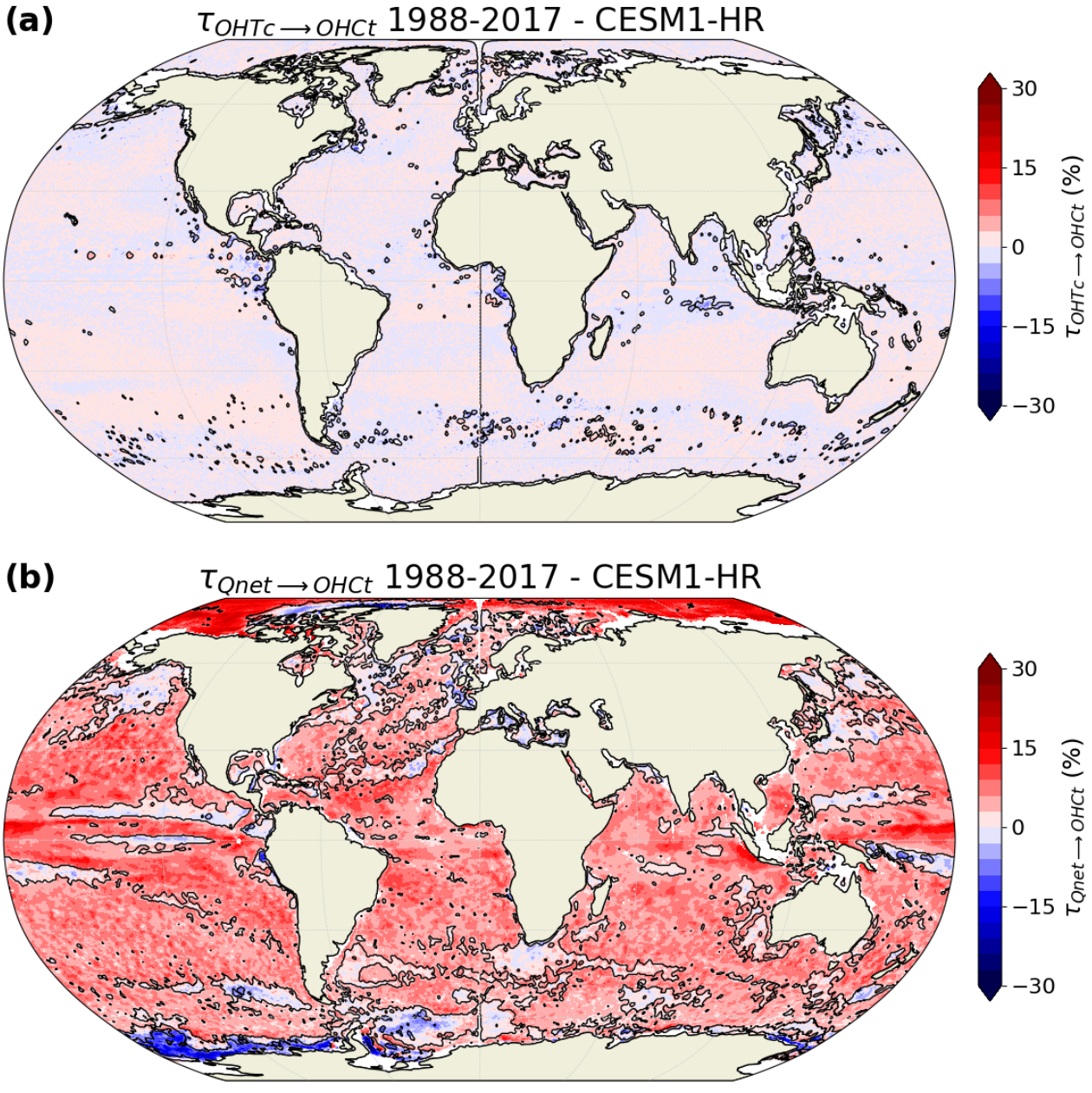

Figure A6. Relative rate of information transfer τ (a) from ocean heat transport convergence (OHTc, upper 50 m) to ocean heat content tendency (OHCt, upper 50 m) and (b) from net surface heat flux (Qnet) to OHCt, based on CESM1-HR. Black contours are drawn around regions with a statistically significant transfer of information (FDR 5%; 500 bootstrap samples; median filter).

https://doi.org/10.5194/egusphere-2022-1340
Preprint. Discussion started: 2 December 2022

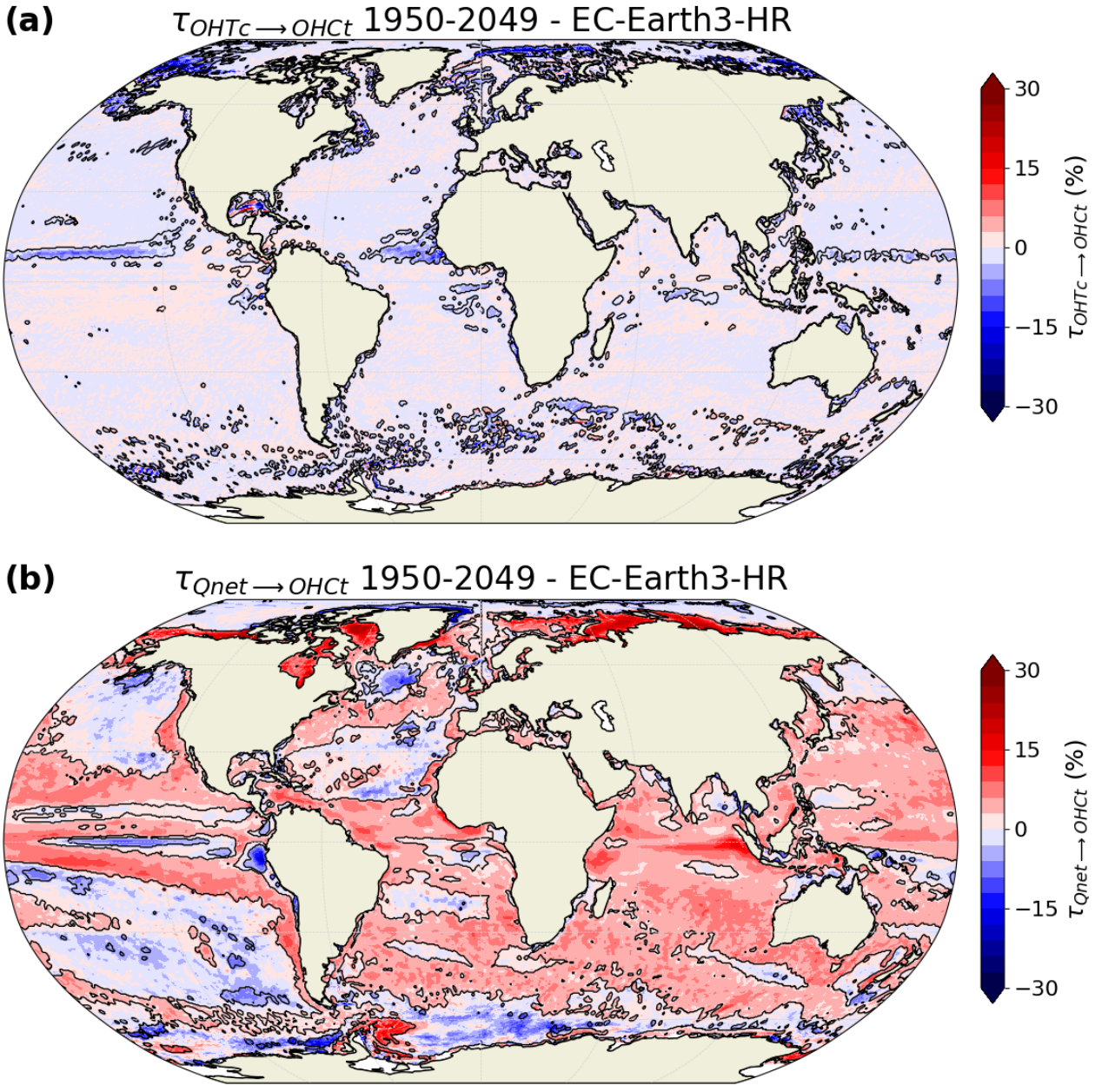

Figure A7. Relative rate of information transfer τ (a) from ocean heat transport convergence (OHTc, upper 50 m) to ocean heat content tendency (OHCt, upper 50 m) and (b) from net surface heat flux (Qnet) to OHCt, based on a 100-year control run with EC-Earth3-HR. Black contours are drawn around regions with a statistically significant transfer of information (FDR 1%; 500 bootstrap samples; median filter).

https://doi.org/10.5194/egusphere-2022-1340
Preprint. Discussion started: 2 December 2022

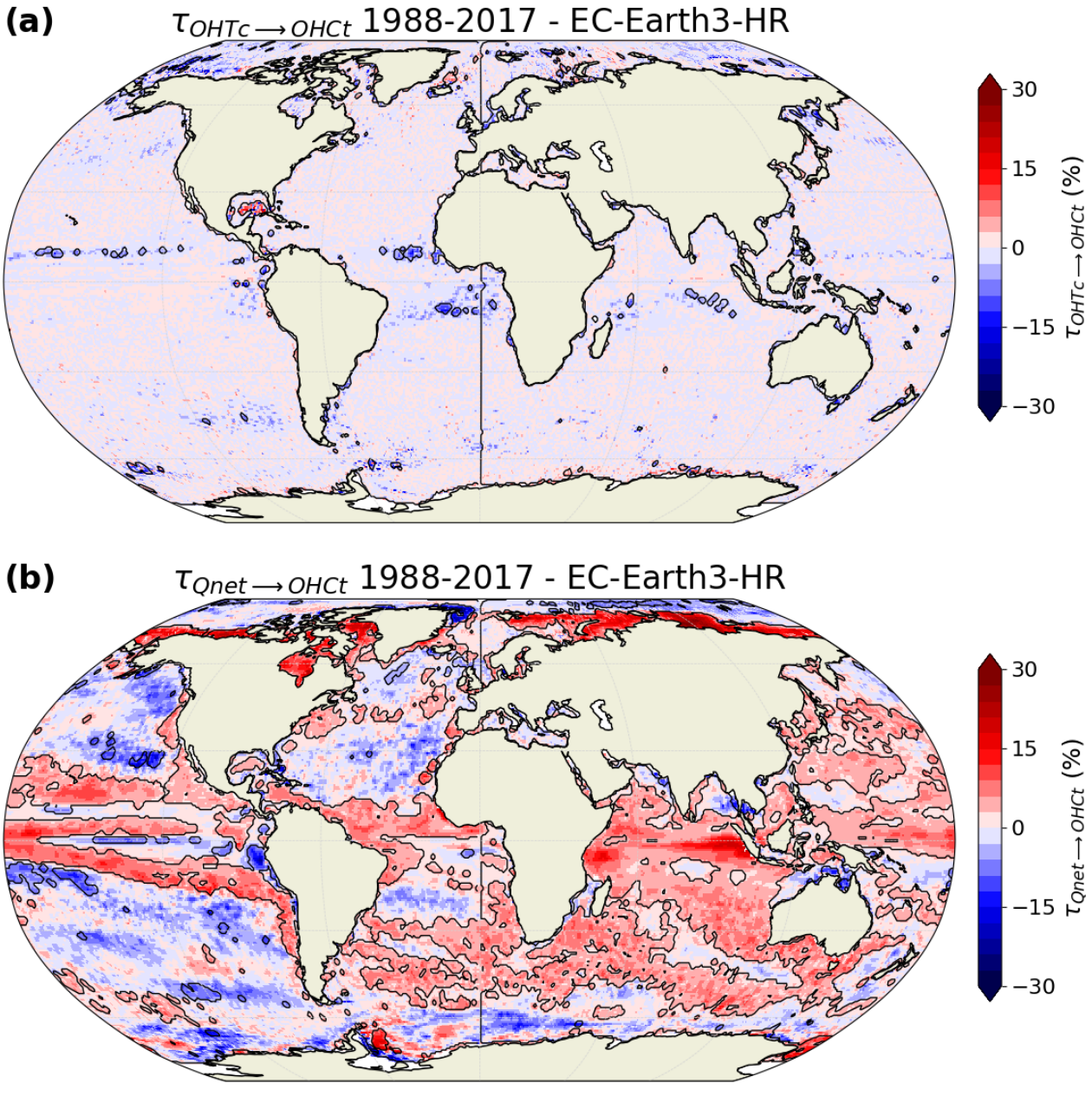

Figure A8. Relative rate of information transfer τ (a) from ocean heat transport convergence (OHTc, upper 50 m) to ocean heat content tendency (OHCt, upper 50 m) and (b) from net surface heat flux (Qnet) to OHCt, based on EC-Earth3-HR with quantities upscaled to EC-Earth3-LR. Black contours are drawn around regions with a statistically significant transfer of information (FDR 5%; 500 bootstrap samples; median filter).

https://doi.org/10.5194/egusphere-2022-1340
Preprint. Discussion started: 2 December 2022

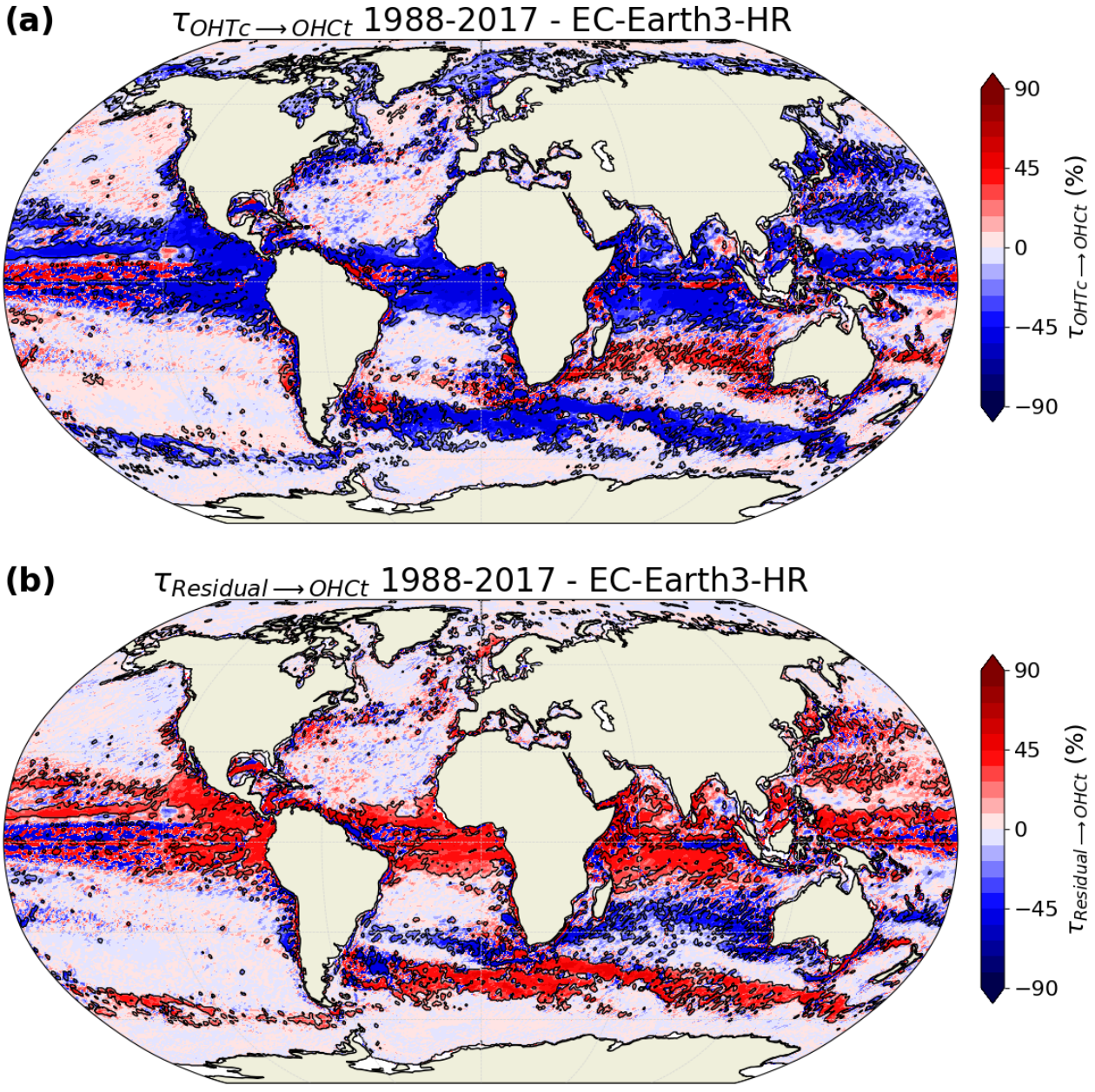

Figure A9. Relative rate of information transfer τ (a) from ocean heat transport convergence (OHTc, upper 50 m) to ocean heat content tendency (OHCt, upper 50 m) and (b) from the residual to OHCt, based on EC-Earth3-HR, omitting net surface heat flux (Qnet). Black contours are drawn around regions with a statistically significant transfer of information (FDR 5%; 500 bootstrap samples; median filter).

https://doi.org/10.5194/egusphere-2022-1340
Preprint. Discussion started: 2 December 2022

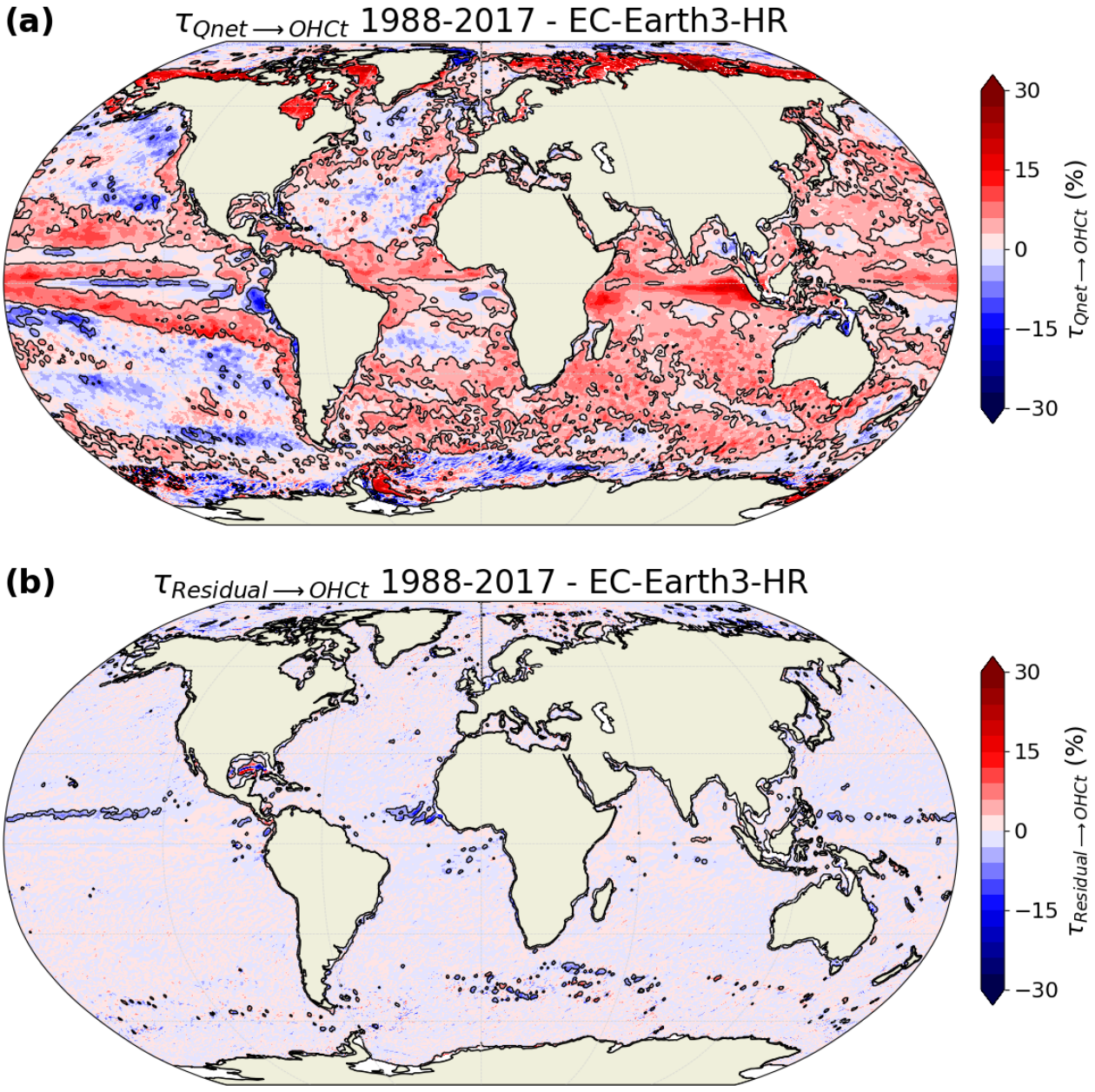

Figure A10. Relative rate of information transfer τ (a) from net surface heat flux (Qnet) to ocean heat content tendency (OHCt, upper 50 m) and (b) from the residual to OHCt, based on EC-Earth3-HR, omitting OHT convergence. Black contours are drawn around regions with a statistically significant transfer of information (FDR 5%; 500 bootstrap samples; median filter).

https://doi.org/10.5194/egusphere-2022-1340
Preprint. Discussion started: 2 December 2022

Author contributions. DD wrote the manuscript with contributions from all co-authors. DD, SV and AB designed the science plan. DD analyzed model outputs and produced the figures. All authors participated in the interpretation of results and provided useful comments to help improve the analysis.

Competing interests. The authors declare that they have no conflict of interest.

Acknowledgements. DD, SV, AB and CF are supported by ROADMAP (Role of ocean dynamics and Ocean-Atmosphere interactions in Driving cliMAte variations and future Projections of impact-relevant extreme events; https://jpi-climate.eu/project/roadmap/), a coordinated JPI-Climate/JPI-Oceans project. DD and SV received funding from the Belgian Federal Science Policy Office under contract B2/20E/P1/ROADMAP. AB received funding from MUR - Italian Ministry of University and Research (D.D. n.1316, 08/06/2021). CF was in part supported by NSF's grant AGS-2040073. We acknowledge the World Climate Research Programme, which, through its Working Group on Coupled Modeling, coordinated and promoted the Coupled Model Intercomparison Project (CMIP6). We thank the climate modeling groups for producing and making available their model output, the Earth System Grid Federation (ESGF) for archiving the data and providing access, and the multiple funding agencies who support CMIP6 and ESGF. Computations have been performed on the ecgate machine of the European Centre for Medium-Range Weather Forecasts (ECMWF) located in Bologna (Italy).

https://doi.org/10.5194/egusphere-2022-1340
Preprint. Discussion started: 2 December 2022

References

Buckley, M. W., Ponte, R. M., Forget, G., and Heimbach, P.: Low-frequency SST and upper-ocean heat content variability in the North Atlantic, Journal of Climate, 27, 4996–5018, https://doi.org/10.1175/JCLI-D-13-00316.1, 2014.

de Boyer Montégut, C., Madex, G., Fischer, A. S., Lazar, A., and Iudicone, D.: Mixed layer depth over the global ocean: An examination of profile data and a profile-based climatology, Journal of Geophysical Research: Oceans, 109, C12 003, https://doi.org/10.1029/2004JC002378, 2004.

Docquier, D.: Liang Index to quantify interactions between ocean heat budget terms (v1.1), Zenodo, https://doi.org/10.5281/zenodo.7358097, 2022.

Docquier, D., Grist, J. P., Roberts, M. J., Roberts, C. D., Semmler, T., Ponsoni, L., Massonnet, F., Sidorenko, D., Sein, D. V., Iovino, D., Bellucci, A., and Fichefet, T.: Impact of model resolution on Arctic sea ice and North Atlantic Ocean heat transport, Climate Dynamics, 53, 4989–5017, https://doi.org/10.1007/s00382-019-04840-y, 2019.

Docquier, D., Vannitsem, S., and Bellucci, A.: The rate of information transfer as a measure of ocean-atmosphere interactions, EGUsphere [preprint], https://doi.org/10.5194/egusphere-2022-942, 2022a.

Docquier, D., Vannitsem, S., Ragone, F., Wyser, K., and Liang, X. S.: Causal links between Arctic sea ice and its potential drivers based on the rate of information transfer, Geophysical Research Letters, 49, e2021GL095 892, https://doi.org/10.1029/2021GL095892, 2022b.

EC-Earth-Consortium: EC-Earth-Consortium EC-Earth3P-HR model output prepared for CMIP6 HighResMIP, https://doi.org/10.22033/ESGF/CMIP6.2323, Earth System Grid Federation, 2018.

EC-Earth-Consortium: EC-Earth-Consortium EC-Earth3P model output prepared for CMIP6 HighResMIP, https://doi.org/10.22033/ESGF/CMIP6.2322, Earth System Grid Federation, 2019.

Fichefet, T. and Morales Maqueda, M. A.: Sensitivity of a global sea ice model to the treatment of ice thermodynamics and dynamics, Journal of Geophysical Research, 102, 12 609–12 646, 1997.

Forster, P., Storelvmo, T., Armour, K., Collins, W., Dufresne, J. L., Frame, D., Lunt, D. J., Mauritsen, T., Palmer, M. D., Watanabe, M., Wild, M., and Zhang, H.: The Earth's Energy Budget, Climate Feedbacks, and Climate Sensitivity. In: Climate Change 2021: The Physical Science Basis. Contribution of Working Group I to the Sixth Assessment Report of the Intergovernmental Panel on Climate Change [Masson-Delmotte, V., P. Zhai, A. Pirani, S. L. Connors, C. Péan, S. Berger, N. Caud, Y. Chen, L. Goldfarb, M. I. Gomis, M. Huang, K. Leitzell, E. Lonnoy, J.B.R. Matthews, T. K. Maycock, T. Waterfield, O. Yelekçi, R. Yu and B. Zhou (eds.) (eds.)], Cambridge University Press, In Press, 2021.

Granger, C. W.: Investigating causal relations by econometric models and cross-spectral methods, Econometrica, 37, 424–438, https://doi.org/10.2307/1912791, 1969.

Grist, J. P., Josey, S. A., New, A. L., Roberts, M. J., Koenigk, T., and Iovino, D.: Increasing Atlantic Ocean heat transport in the latest generation coupled ocean-atmosphere models: The role of air-sea interaction, Journal of Geophysical Research: Oceans, https://doi.org/10.1029/2018JC014387, 2018.

Haarsma, R., Acosta, M., Bakhshi, R., Bretonnière, P.-A., Caron, L.-P., Castrillo, M., Corti, S., Davini, P., Exarchou, E., Fabiano, F., Fladrich, U., Fuentes-Franco, R., Garcia-Serrano, J., von Hardenberg, J., Koenigk, T., Levine, X., Meccia, V. L., van Noije, T., van den Oord, G., Palmeiro, F. M., Rodriguo, M., Ruprich-Robert, Y., Sager, P. L., Tourigny, E., Wang, S., van Weele, M., and Wyser, K.: HighResMIP versions of EC-Earth: EC-Earth3P and EC-Earth3P-HR - description, model computational performance and basic validation, Geoscientific Model Development, 13, 3507–3527, https://doi.org/10.5194/gmd-13-3507-2020, 2020.

https://doi.org/10.5194/egusphere-2022-1340
Preprint. Discussion started: 2 December 2022

Haarsma, R. J., Roberts, M. J., Vidale, P. L., Senior, C. A., Bellucci, A., Bao, Q., Chang, P., Corti, S., Fuckar, N. S., Guemas, V., von Hardenberg, J., Hazeleger, W., Kodama, C., Koenigk, T., Leung, L. R., Lu, J., Luo, J.-J., Mao, J., Mizielinski, M. S., Mizuta, R., Nobre, P., Satoh, M., Scoccimarro, E., Semmler, T., Small, J., and von Storch, J.-S.: High Resolution Model Intercomparison Project (HighResMIP v1.0) for CMIP6, Geoscientific Model Development, 9, 4185–4208, https://doi.org/10.5194/gmd-9-4185-2016, 2016.

Hagan, D. F. T., Wang, G., Liang, X. S., and Dolman, H. A. J.: A time-varying causality formalism based on the Liang–Kleeman information flow for analyzing directed interactions in nonstationary climate systems, Journal of Climate, 32, 7521–7537, https://doi.org/10.1175/JCLI-D-18-0881.1, 2019.

Hurrell, J., Holland, M., Gent, P., Ghan, S., Kay, J., Kushner, P., Lamarque, J.-F., Large, W. G., Lawrence, D., Lindsay, K., Lipscomb, W., Long, M., Mahowald, N. M., Marsh, D., Neale, R., Rasch, P. J., Vavrus, S. J., Vertenstein, M., Bader, D. C., Collins, W. D., Hack, J. J., Kiehl, J., and Marshall, S.: NCAR CESM1-CAM5-SE-LR model output prepared for CMIP6 HighResMIP, https://doi.org/10.22033/ESGF/CMIP6.14262, Earth System Grid Federation, 2020a.

Hurrell, J., Holland, M., Gent, P., Ghan, S., Kay, J., Kushner, P., Lamarque, J.-F., Large, W. G., Lawrence, D., Lindsay, K., Lipscomb, W., Long, M., Mahowald, N. M., Marsh, D., Neale, R., Rasch, P. J., Vavrus, S. J., Vertenstein, M., Bader, D. C., Collins, W. D., Hack, J. J., Kiehl, J., and Marshall, S.: NCAR CESM1-CAM5-SE-HR model output prepared for CMIP6 HighResMIP, https://doi.org/10.22033/ESGF/CMIP6.14220, Earth System Grid Federation, 2020b.

Jiang, S., Hu, H., Lei, L., and Bai, H.: Multi-source forcing effects analysis using Liang–Kleeman information flow method and the community atmosphere model (CAM4.0), Climate Dynamics, 53, 6035–6053, https://doi.org/10.1007/s00382-019-04914-x, 2019.

Kirtman, B. P., Bitz, C., Bryan, F., Collins, W., Dennis, J., Hearn, N., Kinter, J. L., Loft, R., Rousset, C., Siqueira, L., Stan, C., Tomas, R., and Vertenstein, M.: Impact of ocean model resolution on CCSM climate simulations, Climate Dynamics, 39, 1303–1328, https://doi.org/10.1007/s00382-012-1500-3, 2012.

Krakovská, A., Jakubík, J., Chvosteková, M., Coufal, D., Jajcay, N., and Palûs, M.: Comparison of six methods for the detection of causality in a bivariate time series, Physical Review E, 97, 042 207, https://doi.org/10.1103/PhysRevE.97.042207, 2018.

Liang, X. S.: Unraveling the cause-effect relation between time series, Physical Review E, 90, 052 150, https://doi.org/10.1103/PhysRevE.90.052150, 2014.

Liang, X. S.: Information flow and causality as rigorous notions ab initio, Physical Review E, 94, 052 201, https://doi.org/10.1103/PhysRevE.94.052201, 2016.

Liang, X. S.: Normalized multivariate time series causality analysis and causal graph reconstruction, Entropy, 23, 679, https://doi.org/10.3390/e23060679, 2021.

Liang, X. S. and Kleeman, R.: Information transfer between dynamical system components, Physical Review Letters, 95, 244 101, https://doi.org/10.1103/PhysRevLett.95.244101, 2005.

Liang, X. S., Xu, F., Rong, Y., Zhang, R., Tang, X., and Zhang, F.: El Niño Modoki can be mostly predicted more than 10 years ahead of time, Scientific Reports, 11, https://doi.org/110.1038/s41598-021-97111-y, 2021.

Madec, G.: NEMO ocean engine: Note du Pôle de modélisation de l'Institut Pierre-Simon Laplace No 27, http://www.nemo-ocean.eu/About-NEMO/Reference-manuals, 2008.

Madec, G., Bourdallé-Badie, R., Bouttier, P.-A., Bricaud, C., Bruciaferri, D., Calvert, D., Chanut, J., Clementi, E., Coward, A., Delrosso, D., Ethé, C., Flavoni, S., Graham, T., Harle, J., Iovino, D., Lea, D., Lévy, C., Lovato, T., Martin, N., Masson, S., Mocavero, S., Paul, J., Rousset, C., Storkey, D., Storto, A., and Vancoppenolle, M.: NEMO ocean engine. In Note du Pôle de modélisation de l'Institut Pierre-Simon Laplace (IPSL) (v3.6-patch, Number 27), Zenodo, https://doi.org/10.5281/zenodo.3248739, 2017.

https://doi.org/10.5194/egusphere-2022-1340
Preprint. Discussion started: 2 December 2022

Meehl, G. A., Yang, D., Arblaster, J. M., Bates, S. C., Rosenbloom, N., Neale, R., Bacmeister, J., Lauritzen, P. H., Bryan, F., Small, J., Truesdale, J., Hannay, C., Shields, C., Strand, W. G., Dennis, J., and Danabasoglu, G.: Effects of model resolution, physics, and coupling on Southern Hemisphere storm tracks in CESM1.3, Geophysical Research Letters, 46, 12 408–12 416, https://doi.org/10.1029/2019GL084057, 2019.

Palûs, M., Krakovská, A., Jakubík, J., and Chvosteková, M.: Causality, dynamical systems and the arrow of time, Chaos, 28, https://doi.org/10.1063/1.5019944, 2018.

Park, S., Bretherton, C. S., and Rasch, P. J.: Integrating cloud processes in the Community Atmosphere Model, Version 5, Journal of Climate, 27, 6821–6856, https://doi.org/10.1175/JCLI-D-14-00087.1, 2014.

Roberts, C. D., Palmer, M. D., Allan, R. P., Desbruyeres, D. G., Hyder, P., Liu, C., and Smith, D.: Surface flux and ocean heat transport convergence contributions to seasonal and interannual variations of ocean heat content, Journal of Geophysical Research: Oceans, 122, 726–744, https://doi.org/10.1002/2016JC012278, 2017.

Roberts, M.: MOHC HadGEM3-GC31-LL model output prepared for CMIP6 HighResMIP, https://doi.org/10.22033/ESGF/CMIP6.1901, Earth System Grid Federation, 2017a.

Roberts, M.: MOHC HadGEM3-GC31-MM model output prepared for CMIP6 HighResMIP, https://doi.org/10.22033/ESGF/CMIP6.1902, Earth System Grid Federation, 2017b.

Roberts, M.: MOHC HadGEM3-GC31-HM model output prepared for CMIP6 HighResMIP, https://doi.org/10.22033/ESGF/CMIP6.446, Earth System Grid Federation, 2017c.

Roberts, M.: MOHC HadGEM3-GC31-HH model output prepared for CMIP6 HighResMIP, https://doi.org/10.22033/ESGF/CMIP6.445, Earth System Grid Federation, 2018.

Roberts, M. J., Baker, A., Blockley, E. W., Calvert, D., Coward, A., Hewitt, H. T., Jackson, L. C., Kuhlbrodt, T., Mathiot, P., Roberts, C. D., Schiemann, R., Seddon, J., Vannière, B., and Vidale, P. L.: Description of the resolution hierarchy of the global coupled HadGEM3-GC3.1 model as used in CMIP6 HighResMIP experiments, Geoscientific Model Development, 12, 4999–5028, https://doi.org/10.5194/gmd-12-4999-2019, 2019.

Runge, J., Bathiany, S., Bollt, E., Camps-Valls, G., Coumou, D., Deyle, E., Glymour, C., Kretschmer, M., Mahecha, M. D., Munoz-Mari, J., van Nes, E. H., Peters, J., Quax, R., Reichstein, M., Scheffer, M., Scholkopf, B., Spirtes, P., Sugihara, G., Sun, J., Zhang, K., and Zscheischler, J.: Inferring causation from time series in Earth system sciences, Nature Communications, 10, 2553, https://doi.org/10.1038/s41467-019-10105-3, 2019.

Schreiber, T.: Measuring information transfer, Physical Review Letters, 85, 461–464, https://doi.org/10.1103/PhysRevLett.85.461, 2000.

Small, R. J., Bryan, F. O., Bishop, S. P., Larson, S., and Tomas, R. A.: What drives upper-ocean temperature variability in coupled climate models and observations, Journal of Climate, 33, 577–596, https://doi.org/10.1175/JCLI-D-19-0295.1, 2020.

Smith, R. D., Jones, P., Briegleb, B., Bryan, F., Danabasoglu, G., Dennis, J., Dukowicz, J., Eden, C., Fox-Kemper, B., Gent, P., and Hecht, M.: The Parallel Ocean Program (POP) reference manual, Los Alamos National Laboratory Tech. Rep. LAUR-10-01853, 2010.

Stips, A., Macias, D., Coughlan, C., Garcia-Gorriz, E., and Liang, X. S.: On the causal structure between CO2 and global temperature, Scientific Reports, 6, 21 691, https://doi.org/10.1038/srep21691, 2016.

Sugihara, G., May, R., Ye, H., Hsieh, C.-H., Deyle, E., Fogarty, M., and Munch, S.: Detecting causality in complex ecosystems, Science, 338, 496–500, https://doi.org/10.1126/science.1227079, 2012.

Trenberth, K. E. and Caron, J. M.: Estimates of meridional atmosphere and ocean heat transports, Journal of Climate, 14, 3433–3443, https://doi.org/10.1175/1520-0442(2001)014<3433:EOMAAO>2.0.CO;2, 2001.

https://doi.org/10.5194/egusphere-2022-1340
Preprint. Discussion started: 2 December 2022

Vannitsem, S. and Liang, X. S.: Dynamical dependencies at monthly and interannual time scales in the climate system: Study of the North Pacific and Atlantic regions, Tellus A, 74, 141–158, https://doi.org/10.16993/tellusa.44, 2022.

Vannitsem, S., Dalaiden, Q., and Goosse, H.: Testing for dynamical dependence: Application to the surface mass balance over Antarctica, Geophysical Research Letters, 46, 12 125–12 135, https://doi.org/10.1029/2019GL084329, 2019.

Walters, D., Baran, A. J., Boutle, I., Brooks, M., Earnshaw, P., Edwards, J., Furtado, K., Hill, P., Lock, A., Manners, J., Morcrette, C., Mulcahy, J., Sanchez, C., Smith, C., Stratton, R., Tennant, W., Tomassini, L., Van Weverberg, K., Vosper, S., Willett, M., Browse, J., Bushell, A., Dalvi, M., Essery, R., Gedney, N., Hardiman, S., Johnson, B., Johnson, C., Jones, A., Jones, C., Mann, G., Milton, S., Rumbold, H., Sellar, A., Ujiie, M., Whitall, M., Williams, K., and Zerroukat, M.: The Met Office Unified Model Global Atmosphere 7.0/7.1 and JULES Global Land 7.0 configurations, Geoscientific Model Development, 12, 1909–1963, https://doi.org/10.5194/gmd-12-1909-2019, 2019.

Wilks, D. S.: 'The stippling shows statistically significant grid points': How research results are routinely overstated and overinterpreted, and what to do about it, Bulletin of the American Meteorological Society, 97, 2263–2273, https://doi.org/10.1175/BAMS-D-15-00267.1, 2016.

Zuo, H., Balmaseda, M. A., Tietsche, S., Mogensen, K., and Mayer, M.: The ECMWF operational ensemble reanalysis-analysis system for ocean and sea ice: a description of the system and assessment, Ocean Science, 15, 779–808, https://doi.org/10.5194/os-15-779-2019, 2019.